In the present study, through using the spontaneous IAP insertion in mouse *Adamts13* gene, we generated a congenic mouse model that had the distal C-terminally truncated ADAMTS13 on 129/Sv genetic background. While comparing with wild-type 129/Sv mice having full-length ADAMTS13 and ADAMTS13-deficient mice on the same genetic background, we analyzed platelet thrombus formation in the congenic mice to define physiologic significance of the distal C-terminal domains in ADAMTS13 functions. Our results indicate that the distal C-terminal domains of ADAMTS13 contribute to the processing of VWF multimers in vivo, and that the importance of these domains becomes obvious after suffering thrombogenic stimuli.

Methods

Animals

The 129/Sv mice were purchased from Clea Japan (Tokyo, Japan). C57BL/6 mice were purchased from Japan SLC (Hamamatsu, Japan). ADAMTS13-deficient mice on the 129/Sv genetic background were described previously.[17,18] ADAMTS13-congenic mice were developed by introgressing the C57BL/6-*Adamts13* gene onto the 129/Sv genetic background, as follows. C57BL/6 mice were backcrossed to 129/Sv mice for 10 generations while retaining the C57BL/6-*Adamts13* gene. In the resulting N10 heterozygous mice, autosomal chromosomes were theoretically 99.9% identical to those of the 129/Sv strain and sex chromosomes were derived exclusively from the 129/Sv strain. The N10 heterozygous mice were interbred to produce homozygous mice. The *Adamts13*-genotype was determined by polymerase chain reaction (PCR) with HotStarTaq DNA polymerase (QIAGEN, Hilden, Germany). The amplification was carried out using primers: the intron 23-specific forward primer, 5′-ACCTCTCAAGTGTTTGGGATGCTA-3′, the IAP-specific reverse primer, 5′-TCAGCGCCATCTTGTGACGGCGAA-3′, and the primer downstream of the IAP target site, 5′-TGCCAGATGGCCATGATTAACTCT-3′. For the experiments, all animals were matched for age and sex. All animal procedures were approved by the Animal Care and Use Committees of the National Cardiovascular Center Research Institute and Immune Disease Institute.

Northern blot analysis

Total RNA was extracted from liver using ISOGEN reagent (Nippon Gene, Tokyo, Japan) and poly(A)$^+$ RNA was purified using PolyATtract mRNA Isolation Systems (Promega, Madison, WI). The alkaline phosphatase–labeled probe was synthesized from mouse *Adamts13* cDNA (1.3 kb) using AlkPhos Direct labeling module (GE Healthcare, Little Chalfont, United Kingdom). Poly(A)$^+$ RNA was separated on a 1% agarose gel containing 2% formaldehyde and transferred to a nylon membrane. The probe was hybridized to the blot and detected using CDP-Star detection reagent (GE Healthcare).

Blood sampling

Blood was collected from the retro-orbital plexus into tubes containing a 0.1 volume of 3.8% sodium citrate. Blood cell counts and hematocrit were determined using an automatic cell counter (KX-21NV; Sysmex, Kobe, Japan). Plasma was prepared from blood by centrifugation at 800*g* for 15 minutes.

Determination of plasma ADAMTS13 activity

Plasma ADAMTS13 activity was measured using GST-mVWF73-H, a recombinant mouse VWF73 peptide flanked by N-terminal glutathione S-transferase (GST) and C-terminal His_6 tags, as described previously.[14] In brief, GST-mVWF73-H (500 ng) was incubated with 0.8 μL plasma in 40 μL reaction buffer (10 mM *N*-2-hydroxyethylpiperazine-*N*′-2-ethanesulfonic acid, 150 mM NaCl, 5 mM $CaCl_2$, and 0.005% Tween 20, pH 7.4) at 37°C for 1 hour. The reaction was stopped by adding 10 μL sodium dodecyl sulfate (SDS) sample buffer (50 mM tris(hydeoxymethyl)aminomethane-HCl, 10 mM EDTA, 10% SDS, 250 mM dithiothreitol, 30% glycerol, and 0.1% bromophenol blue, pH 6.8). The samples were subjected to SDS–polyacrylamide gel electrophoresis and Western blot using a rabbit anti-GST antibody (Invitrogen, Carlsbad, CA) and a peroxidase-labeled anti–rabbit IgG antibody (KPL, Gaithersburg, MD). Activity was also determined using a fluorogenic human VWF73 peptide of FRETS-VWF73 (Peptide Institute, Minoh, Japan).[19,20] FRETS-VWF73 (2 μM) was incubated with 4 μL plasma in 200 μL assay buffer (5 mM bis(2-hydroxyethyl)-amino-tris(hydeoxymethyl)methane, 25 mM $CaCl_2$, and 0.005% Tween 20, pH 6.0) at 30°C. Increases in fluorescence were measured using a 350-nm excitation filter and a 440-nm emission filter in a fluorescence photometer (Mx3000P; Stratagene, La Jolla, CA).

VWF multimer analysis

Plasma VWF multimer patterns were analyzed as described previously.[17] Plasma samples in SDS sample buffer were electrophoresed on a 1% agarose gel (Agarose IEF; GE Healthcare) at a constant current of 15 mA at 4°C. After transfer to a nitrocellulose membrane, the membrane was incubated in peroxidase-conjugated rabbit anti–human VWF (1:500; Dako, Glostrup, Denmark) in 5% skim milk to detect VWF multimers. Bound antibody was detected with Western Lighting Chemiluminescence Reagent Plus (PerkinElmer, Waltham, MA) on an image analyzer (LAS-3000; Fujifilm, Tokyo, Japan). The chemiluminescent intensities of each lane were scanned using Image Gauge software (version 4.2.2; Fujifilm); the relative intensity profiles were shown.

Parallel plate flow chamber assay

Platelet thrombus formation in flowing blood on immobilized collagen was analyzed using a parallel plate flow chamber as described previously.[17,21] Acid-insoluble type I collagen–coated glass coverslips were placed in a flow chamber. The chamber was mounted on a fluorescence microscope (Axiovert 200M; Carl Zeiss, Oberkochen, Germany) equipped with a CCD camera system (DXC-390; Sony, Tokyo, Japan). Blood was collected into tubes containing argatroban (240 μM; Mitsubishi Chemical, Tokyo, Japan). The fluorescent dye mepacrine (10 μM; Sigma-Aldrich, St Louis, MO) was added to the blood. Whole blood samples were aspirated through the chamber and across the collagen-coated coverslip at a constant wall shear rate. To analyze the cumulative thrombus volume, image sets at 1.0-μm z-axis intervals within a defined area (156.4 μm × 119.6 μm) were captured using MetaMorph software (version 6.1.4; Universal Imaging, West Chester, PA). After blind deconvolution of image sets processed by AutoDeblur software package (version 8.0.2; AutoQuant Imaging, Troy, NY), 3D volumetric measurements of thrombi were accomplished using VoxBlast software (version 3.0; Vartek, Fairfield, IA).

Intravital microscopy

Intravital microscopy was performed as described previously.[22,23] Platelets were isolated from platelet-rich plasma and fluorescently labeled with calcein AM (2.5 μg/mL; Invitrogen). Recipient mice were anesthetized and labeled platelets were infused through retro-orbital plexus. The mesentery was gently exteriorized through a midline abdominal incision and arterioles of 100- to 150-μm diameters were visualized with a fluorescence microscope and a CCD camera system. The shear rate was calculated using an optical Doppler velocimeter as described.[24] Filter paper saturated with 10% ferric chloride was applied for 5 minutes on an arteriole by topical application. Thrombus formation in the arteriole was monitored for 40 minutes after injury or until complete occlusion occurred and lasted for more than 30 seconds. The following 2 parameters were evaluated: time to first thrombus formation, defined as the time required for formation of a thrombus larger than 30 μm, and occlusion time, defined as the time required for cessation of blood flow for at least 30 seconds.

Collagen plus epinephrine–induced thrombosis model

A mixture of 600 ng/g collagen (Nycomed, Roskilde, Denmark) and 60 ng/g epinephrine (Sigma-Aldrich) was infused into tail vein of mice.[17,25]

Blood was collected 5 minutes after the infusion and platelet counts were determined.

Statistical analysis

Statistical significance was assessed by the one-way analysis of variance followed by the Bonferroni multiple comparison tests. Differences were considered to be significant at P values less than .05.

Results

Generation of Adamts13$^{S/S}$ mice

To address the functional implication of the distal C-terminal domains of ADAMTS13 in vivo, we generated and characterized a congenic mouse model that has the C-terminally truncated form of ADAMTS13 on 129/Sv genetic background (Figure 1A). We confirmed the presence of IAP insertion in the *Adamts13* gene of the congenic (*Adamts13*$^{S/S}$) mice by PCR (data not shown) and detected an IAP chimeric transcript (~ 3.5 kb) by Northern blotting of RNA from liver (Figure 1B), primary site of synthesis.[14] An IAP-free ADAMTS13 mRNA (~ 5 kb) was detected in wild-type 129/Sv (*Adamts13*$^{L/L}$) mice and no ADAMTS13 mRNA was detected in ADAMTS13-deficient (*Adamts13*$^{-/-}$) mice on 129/Sv genetic background (Figure 1B). *Adamts13*$^{S/S}$ mouse plasma exhibited higher cleaving activity for both GST-mVWF73-H and FRETS-VWF73 than *Adamts13*$^{L/L}$ mouse plasma, whereas the activity in *Adamts13*$^{-/-}$ mouse plasma was below detection limits (Figure 1C,D). Therefore, the distal C-terminal domains of ADAMTS13 were not necessary for the cleavage of the VWF73-based peptide substrate as observed previously.[8,14] Platelet counts were not different among the genotypes (*Adamts13*$^{L/L}$, 744 ± 180 × 10^9/L; *Adamts13*$^{S/S}$, 693 ± 44 × 10^9/L; *Adamts13*$^{-/-}$, 672 ± 39 × 10^9/L; mean ± SD, n = 8). Both *Adamts13*$^{S/S}$ mice and *Adamts13*$^{-/-}$ mice were viable and showed no TTP-like symptoms throughout the study.

Adamts13$^{S/S}$ mice have normal VWF multimers

As previously reported,[17] UL-VWF multimers persisted in plasma of *Adamts13*$^{-/-}$ mice on 129/Sv-genetic background (Figure 2). Thus, ADAMTS13 activity is important for the size regulation of VWF multimers in mice at least on this genetic background. However, the VWF multimer patterns in *Adamts13*$^{S/S}$ mice were indistinguishable from those in *Adamts13*$^{L/L}$ mice (Figure 2). These results suggest that the distal C-terminally truncated form of mouse ADAMTS13 exhibits VWF-cleaving activity sufficient for maintenance of normal size distribution of plasma VWF multimers under steady state in vivo.

In vitro thrombogenesis is increased in *Adamts13*$^{S/S}$ mice only at a high shear rate

When whole blood was perfused over a collagen-coated surface in a parallel plate flow chamber at a shear rate of 1000 s^{-1}, platelet thrombus formation was significantly promoted in *Adamts13*$^{-/-}$ mice (Figure 3A) compared with *Adamts13*$^{L/L}$ mice, consistent with the presence of UL-VWF multimers in plasma of *Adamts13*$^{-/-}$ mice. However, whole blood thrombus formation at 1000 s^{-1} was not significantly different between *Adamts13*$^{S/S}$ mice and *Adamts13*$^{L/L}$ mice (Figure 3A), indicating that the distal C-terminally truncated form of mouse ADAMTS13 does not completely lose the activity.

As fluid shear rate increases progressively, the interaction between VWF and platelet GPIbα becomes more important in platelet thrombus formation.[26] It has been reported that thrombus formation in mouse blood on collagen surface is completely dependent on the VWF-GPIbα interaction above a threshold shear rate between 2000 s^{-1} and 5000 s^{-1}.[27] In addition, ADAMTS13 cleaves VWF and down-regulates thrombus formation in shear rate–dependent manner.[28] Based on these observations, we further examined thrombus formation at a higher shear rate of 5000 s^{-1}. As expected, thrombus formation in *Adamts13*$^{-/-}$ mice was significantly elevated compared with *Adamts13*$^{L/L}$ mice at 5000 s^{-1} (Figure 3B). In addition, we found accelerated thrombus formation in *Adamts13*$^{S/S}$ mice compared with *Adamts13*$^{L/L}$ mice at this higher shear rate (Figure 3B). These results suggest that the distal C-terminally truncated form of mouse ADAMTS13 has reduced

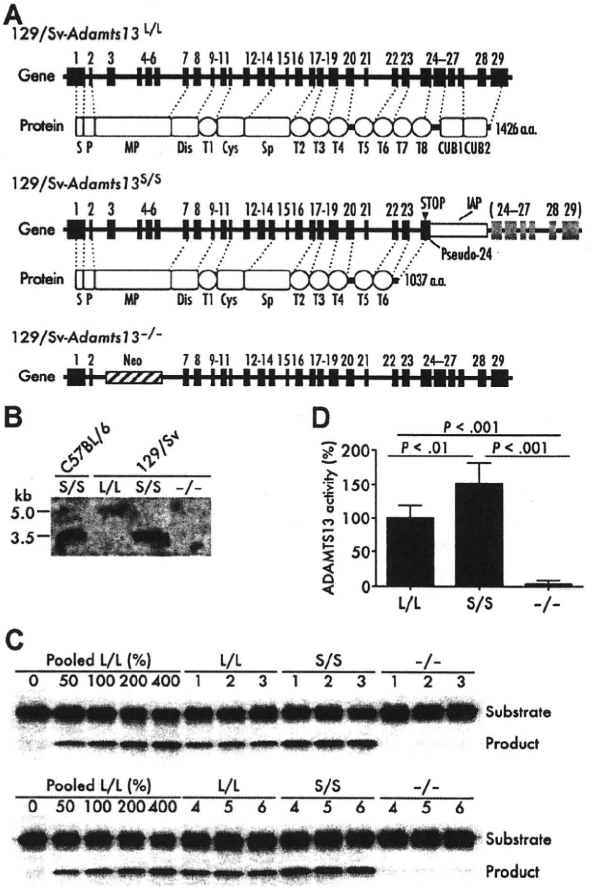

Figure 1. Generation of *Adamts13*$^{S/S}$ mice with 129/Sv-genetic background. (A) Gene and protein structure of ADAMTS13 in the wild-type (*Adamts13*$^{L/L}$) 129/Sv mice, the *Adamts13*$^{S/S}$ mice on 129/Sv genetic background, and the *Adamts13*$^{-/-}$ mice on 129/Sv genetic background. An intracisternal A-particle (*IAP*) insertion into intron 23 creates a pseudo-exon 24 including a premature stop codon. ADAMTS13 with a truncated C-terminus is expressed mainly in *Adamts13*$^{S/S}$ mice. S indicates signal peptide; P, propeptide; MP, metalloprotease domain; Dis, disintegrin-like domain; T (numbered 1-8), thrombospondin type 1 motif domain; Cys, cysteine-rich domain; Sp, spacer domain; and CUB, complement components C1r/C1s, urchin epidermal growth factor, and bone morphogenic protein-1 domain. (B) Expression of *Adamts13* mRNA in liver. Poly(A)$^+$ RNA isolated from liver of indicated mice was probed with a 1.3-kb Adamts13 cDNA corresponding to exons 3 to 13. (C) GST-mVWF73-H assay. Plasma ADAMTS13 activity of indicated mice was measured using a recombinant mouse VWF73 peptide, GST-mVWF73-H. Results from 6 mice for each genotype are shown. Standard reactions using graded amounts of pooled plasma from 10 *Adamts13*$^{L/L}$ mice were performed simultaneously. (D) FRETS-VWF73 assay. Plasma ADAMTS13 activity in indicated mice was determined using a fluorogenic human VWF73 peptide, FRETS-VWF73. Data are mean ± SD of 6 mice for each genotype. The average activity measured in *Adamts13*$^{L/L}$ mice was arbitrarily defined as 100%.

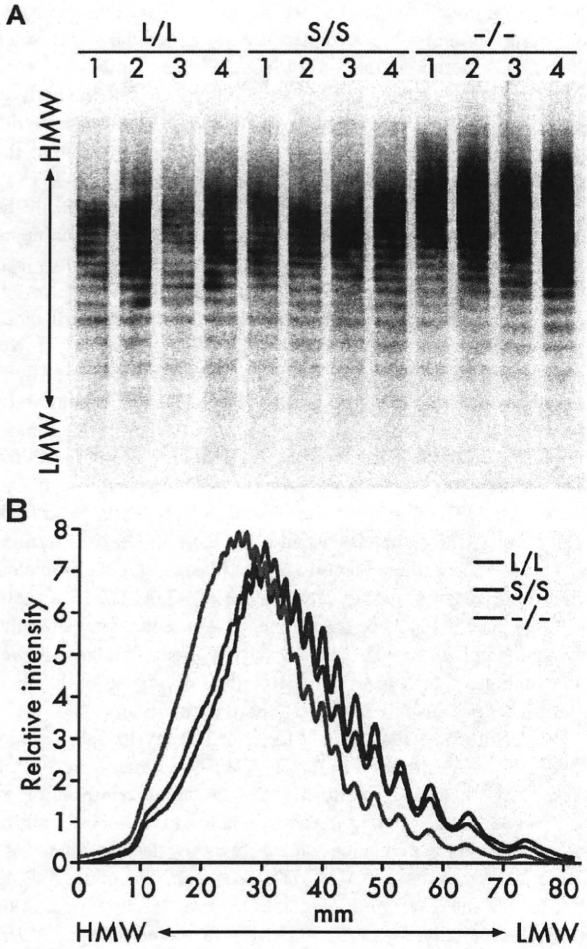

Figure 2. Plasma VWF multimers. (A) VWF multimer patterns. Plasma samples (1 μL/lane) from *Adamts13*$^{L/L}$, *Adamts13*$^{S/S}$, and *Adamts13*$^{-/-}$ mice were electrophoresed on SDS-agarose gels and transferred to nitrocellulose membranes. VWF multimers were detected with anti-VWF antibodies. (B) Relative intensities of plasma VWF multimers. The chemiluminescent intensities of the VWF multimer patterns (A) were scanned using image analysis software. An average of multiple lanes from 4 mice for each genotype is shown. HMW indicates high molecular weight; LMW, low molecular weight.

activity compared with the full-length form and does not sufficiently limit thrombus formation under high shear rate in vitro.

In vivo thrombus growth is accelerated in *Adamts13*$^{S/S}$ mice

To examine whether the truncation of the distal C-terminal domains in ADAMTS13 affects thrombus formation in vivo, we carried out intravital microscopy experiments in a model of experimental arteriolar thrombosis. In this model, vascular injury was induced by topical application of ferric chloride on a mesenteric arteriole, which provoked the generation of free radicals leading to the endothelial disruption.[23] The diameter and shear rate of studied arterioles were 118.0 plus or minus 13.1 μm and 1362 plus or minus 219 s^{-1} (mean ± SD, n = 16) for *Adamts13*$^{L/L}$ mice, 122.8 plus or minus 11.1 μm and 1394 plus or minus 136 s^{-1} (n = 16) for *Adamts13*$^{S/S}$ mice, and 115.6 plus or minus 10.8 μm and 1405 plus or minus 225 s^{-1} (n = 12) for *Adamts13*$^{-/-}$ mice and not significantly different among the groups. Both time to first thrombus (Figure 4A) and occlusion time (Figure 4B) after injury in *Adamts13*$^{-/-}$ mice (time to first thrombus = 5.1 ± 1.9 minutes, occlusion time = 9.2 ± 1.6 minutes; mean ± SD) were signifi-

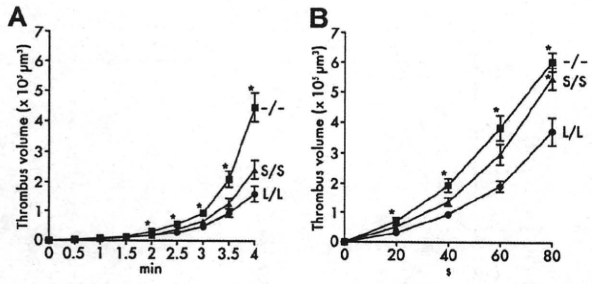

Figure 3. In vitro thrombogenesis on collagen surface under flow. (A) Thrombus formation at 1000 s^{-1}. Whole blood from *Adamts13*$^{L/L}$, *Adamts13*$^{S/S}$, or *Adamts13*$^{-/-}$ mice containing mepacrine-labeled platelets was perfused over an acid-insoluble type I collagen–coated surface at a wall shear rate of 1000 s^{-1}. The cumulative thrombus volume, analyzed using a multidimensional imaging system, was measured every 0.5 minutes until 4 minutes. Data are the mean ± SEM of 25 mice for each genotype. (B) Thrombus formation at 5000 s^{-1}. Whole-blood samples from indicated mice were perfused over an acid-insoluble type I collagen–coated surface at a wall shear rate of 5000 s^{-1}. The cumulative thrombus volume was measured every 20 seconds until 80 seconds. Blood from 2 mice was pooled and used for experiments. Data are the mean ± SEM of 15 samples for each genotype. *$P < .05$ in comparison with *Adamts13*$^{L/L}$ mice.

cantly decreased compared with *Adamts13*$^{L/L}$ mice (time to first thrombus = 7.8 ± 1.3 minutes, occlusion time = 15.3 ± 3.6 minutes), indicating that ADAMTS13 contributes to down-regulation of thrombogenesis at the site of arteriolar injury in 129/Sv mice. In the case of *Adamts13*$^{S/S}$ mice, time to first thrombus after injury (7.6 ± 1.2 minutes) was not different from *Adamts13*$^{L/L}$ mice. However, the initial thrombi grew rapidly to occlusive size in *Adamts13*$^{S/S}$ mice and occlusion time was significantly shorter in *Adamts13*$^{S/S}$ mice (12.5 ± 1.9 minutes) compared with *Adamts13*$^{L/L}$ mice (Figure 4B). These results suggest that the distal C-terminally truncated form of mouse ADAMTS13 is less active in down-regulating thrombus growth in vivo compared with full-length ADAMTS13.

To elucidate the consequences of the lack of the distal C-terminal domains in ADAMTS13 on systemic thrombosis, we performed collagen plus epinephrine infusion model experiments. In this model, widespread intravascular thrombosis was induced by intravenous infusion of collagen fibrils in combination with epinephrine, and the incorporation of platelets into thrombi was monitored by the reduction in circulating platelet counts.[29] Consistent with our previous observation,[17] platelet counts after the infusion were significantly lower in *Adamts13*$^{-/-}$ mice

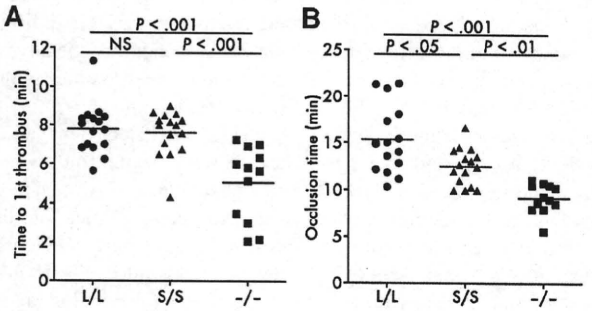

Figure 4. In vivo thrombogenesis in ferric chloride–injured mesenteric arterioles. (A) Time to first thrombus formation. Calcein AM–labeled platelets representing approximately 2.5% of total platelets were observed in mesenteric arterioles of live mice after injury with 10% ferric chloride. The time required for formation of a thrombus more than 30 μm was measured. (B) Occlusion time. The time required for a complete stop of blood flow was measured after injury with 10% ferric chloride. Symbols represent data from a single mouse. Bars represent the mean values of groups (n = 16 for *Adamts13*$^{L/L}$ mice, n = 16 for *Adamts13*$^{S/S}$ mice, and n = 12 for *Adamts13*$^{-/-}$ mice).

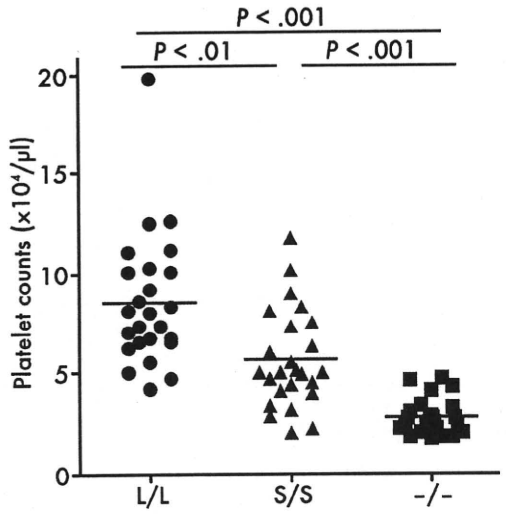

Figure 5. Platelet counts after collagen plus epinephrine infusion. Mice were injected with 600 ng/g collagen plus 60 ng/g epinephrine via tail vein and platelet counts were measured 5 minutes after injection. Symbols represent platelet counts from a single mouse. Bars represent the mean values of 25 mice in each group. Platelet counts of untreated mice were not different among the groups.

($28 \pm 8 \times 10^9$/L, mean ± SD) than in *Adamts13*$^{L/L}$ mice ($85 \pm 33 \times 10^9$/L), suggesting that ADAMTS13 contributes to inhibition of platelet aggregation in this experimental system (Figure 5). Platelet counts after the infusion in *Adamts13*$^{S/S}$ mice ($56 \pm 24 \times 10^9$/L) were significantly higher than in *Adamts13*$^{-/-}$ mice and lower than in *Adamts13*$^{L/L}$ mice (Figure 5), whereas platelet counts of untreated mice were not different among the groups (*Adamts13*$^{L/L}$, $666 \pm 44 \times 10^9$/L; *Adamts13*$^{S/S}$, $770 \pm 65 \times 10^9$/L; *Adamts13*$^{-/-}$, $710 \pm 49 \times 10^9$/L, mean ± SD of 4 mice). These findings complement accelerated thrombus growth in *Adamts13*$^{S/S}$ mice compared with *Adamts13*$^{L/L}$ mice, indicating that the distal C-terminally truncated form of mouse ADAMTS13 has significantly reduced activity in vivo.

Discussion

It is now evident that genetic background is an important phenotypic determinant in mutant mice with hemostatic defects. For instance, mice carrying the factor V Leiden (R504Q) mutation have shown increased perinatal thrombotic mortality on the mixed 129/Sv and C57BL/6J background relative to C57BL/6J background.[30] Similar effects of genetic backgrounds on phenotypes have been observed in other mutants such as the thrombomodulin G404P-mutant mice,[31] the fibrinogen-deficient mice,[32] and the tissue factor–deficient mice.[33] In ADAMTS13-deficient mice, genetic backgrounds have also been shown to significantly affect their thrombotic phenotypes.[34] Thus, phenotypes of ADAMTS13 mutant mice should be compared with control mice on the appropriate and uniform strain background. We have previously demonstrated that ADAMTS13 deficiency in mice results in a prothrombotic state with accumulation of UL-VWF multimers on 129/Sv background.[17] Therefore in this study, we applied a spontaneous mutation in the *Adamts13* gene of C57BL/6 mice onto 129/Sv mice by 10-generation backcrossing, and obtained the congenic mice that were expected to have 99.9% 129/Sv genome and primarily expressed the distal C-terminally truncated ADAMTS13. Then, we compared their phenotypes with positive and negative control animals: the wild-type 129/Sv mice and the 129/Sv-background ADAMTS13-deficient mice. By this approach, we minimized the background effects and defined the significance of the distal C-terminal domains of ADAMTS13 in mice.

Plasma of the congenic mice exhibited higher cleaving activity against GST-mVWF73-H and FRETS-VWF73 compared with plasma of the wild-type mice. We previously observed that the recombinant distal C-terminally truncated mouse ADAMTS13 cleaves GST-mVWF73-H to a similar extent compared with the full-length form.[14] The other group reported that the recombinant distal C-terminally truncated mouse ADAMTS13 is slightly less active in cleaving GST-mVWF73-H than the full-length form.[15] These findings suggest that the distal C-terminally truncated ADAMTS13 in mouse plasma has equivalent or slightly lower specific activity against VWF73-based substrates compared with the full-length ADAMTS13. Thus, the data in the present study imply that the distal C-terminally truncated ADAMTS13 is more abundant than the full-length form in circulating blood in 129/Sv mice. Preferential expression of the distal C-terminally truncated mouse ADAMTS13 has also been found in HeLa cells[14] and HEK 293T cells.[15] Unfortunately, because we have failed to determine the ADAMTS13 antigen levels in mouse plasma, it remains unclear whether the distal C-terminal truncation of ADAMTS13 actually increases plasma levels of the enzyme. Despite the congenic mice having higher in vitro ADAMTS13 activity in plasma, they showed prothrombotic phenotypes, suggesting the importance of the distal C-terminal domains in ADAMTS13 activity in vivo.

We reconfirmed that ADAMTS13 deficiency in 129/Sv mice allowed the accumulation of UL-VWF multimers in plasma (Figure 2), therefore, promising the essential contribution of ADAMTS13 on preventing the accumulation of UL-VWF multimers in 129/Sv mice. Under these situations, lack of the distal C-terminal domains of ADAMTS13 in 129/Sv mice did not increase plasma VWF multimer sizes (Figure 2), showing that the distal C-terminally truncated ADAMTS13 maintained the VWF-cleaving activity in vivo. Although the distal C-terminally truncated form of mouse ADAMTS13 was reported to show considerably lower activity than the full-length form for purified human VWF multimers under in vitro static conditions,[15] our results show that the distal C-terminal truncation of mouse ADAMTS13 allows retention of normal size distribution of plasma VWF multimers in vivo at least under steady state.

In the parallel-plate flow chamber experiments, ADAMTS13 deficiency in 129/Sv mice markedly enhanced thrombogenic responses (Figure 3), indicating that ADAMTS13 is critical for limiting platelet thrombus formation under whole blood flow conditions. In the same experimental conditions, the distal C-terminal truncation of ADAMTS13 in 129/Sv mice did not promote thrombogenesis at 1000 s^{-1} (Figure 3A) but significantly promoted thrombogenesis at 5000 s^{-1} (Figure 3B). It is conceivable that the distal C-terminally truncated ADAMTS13 is active but not fully competent to cleave VWF within growing thrombus under flow. Because both the interaction of GPIbα-VWF and the cleavage of VWF by ADAMTS13 are facilitated by increasing fluid shear rate, the function of the distal C-terminal domains may become vital to down-regulate thrombogenesis under high shear conditions. Actually, similar results were obtained in the in vivo arteriolar injury model experiments (Figure 4). The distal C-terminal truncation of ADAMTS13 in 129/Sv mice did not affect the time to first thrombus formation in the arterioles where fluid shear rates were around 1500 s^{-1} (Figure 4A). However, when thrombus grew to a larger size, the arteriolar lumen was narrowed, which resulted in increase in shear rates.[23] Then, the distal C-terminal truncation of

ADAMTS13 significantly reduced the occlusion time compared with full-length ADAMTS13 (Figure 4B). Therefore, the distal C-terminal domains are important for ADAMTS13 to sufficiently down-regulate thrombogenesis under high shear rate in vivo as well as in vitro. After the induction of systemic platelet aggregation by challenge with a mixture of collagen and epinephrine, consumptive thrombocytopenia was also enhanced by the distal C-terminal truncation of ADAMTS13 in 129/Sv mice (Figure 5), supporting the idea that the distal C-terminal domains are required for optimal down-regulation of platelet aggregation in vivo. The complete deficiency of ADAMTS13 in 129/Sv significantly accelerated thrombus growth to injured vessel wall and systemic thrombi compared with 129/Sv mice with truncation of the distal C-terminal domains in ADAMTS13 (Figures 4,5). Therefore, we can conclude that the distal C-terminally truncated ADAMTS13 has significantly decreased activity in limiting thrombosis in vivo.

The binding of platelets to VWF is reported to accelerate the cleavage of VWF by ADAMTS13 under static[35] and flow[36] conditions in vitro. It has also been shown that ADAMTS13 can cleave platelet-bound VWF multimers[37] and limit thrombus formation through the cleavage of VWF at the surface of forming thrombi[28] in in vitro flow chamber systems. Therefore, in our experimental settings, ADAMTS13 attenuates thrombus growth, possibly through the cleavage of VWF multimers bound on the surface of platelet-rich thrombi under high shear rate. The distal C-terminal domains may be necessary for ADAMTS13 to efficiently recognize and cleave platelet-bound VWF multimers on a growing thrombus. Conceivably, the distal C-terminal domains may contribute to the interaction with unidentified ADAMTS13-binding cofactors localized on the surface of platelets or subendothelium, and this interaction may be necessary for ADAMTS13 to control VWF-mediated thrombus formation. However, we cannot rule out the possibility that the distal C-terminal domains of ADAMTS13 contribute to the prevention of thrombosis independent from the VWF-cleaving activity of ADAMTS13, nevertheless VWF has been suggested as the only relevant substrate for ADAMTS13[38] and functions of ADAMTS13 other than its VWF-cleaving activity have yet to be reported.

The distal C-terminally truncated ADAMTS13 is expressed in a lot of mouse strains including the BALB/c, C3H/He, C57BL/6, and DBA/2 strains as substitute for the full-length form.[14,15] Our present results suggest that thrombotic response in these strains would be increased, at least partially, by their incomplete ADAMTS13 activity. This should be taken into account when studying genetically modified mice with heterogeneous genetic background.

In summary, our results define the role of the distal C-terminal domains in ADAMTS13 in vivo. Deletion of the C-terminal 2 Tsp1 and 2 CUB domains permits normal size distribution of plasma VWF multimers under steady state, but exacerbates platelet thrombosis after thrombogenic stimulation in mice. Thus, the distal C-terminally truncated ADAMTS13 is not fully active in vivo. These distal C-terminal domains of ADAMTS13 may play a role in the efficient processing of VWF multimers during platelet thrombus growth, and thus their functions may become increasingly important when vascular damage is induced.

Acknowledgments

We thank Ms Miyuki Kuroi and Ms Yuko Nobe (National Cardiovascular Center Research Institute), and Ms Meghan Walsh (Immune Disease Institute) for technical assistance.

This work was supported in part by grants-in-aid from the Ministry of Health, Labor, and Welfare of Japan, Tokyo, Japan (T.M.); the Ministry of Education, Culture, Sports, Science, and Technology of Japan, Tokyo, Japan (F.B., K.K., and T.M.); the Japan Society for the Promotion of Science, Tokyo, Japan (K.K. and T.M.); and from the Program for Promotion of Fundamental Studies in Health Sciences of the National Institute of Biochemical Innovation of Japan, Ibaraki, Japan (T.M.); a Sponsored Research Agreement from Baxter Bioscience, Vienna, Austria (A.K.C. and D.D.W.) and a National Heart, Lung, and Blood Institute of the National Institutes of Health grant P01-HL066105 (D.D.W.).

Authorship

Contribution: F.B. designed research, performed experiments, analyzed data, and wrote the paper; A.K.C. performed experiments, contributed vital analytical tools, and analyzed the data; K.K. designed research, performed experiments, and wrote the paper; J.Y. performed experiments and analyzed data; S.M. and D.D.W. contributed vital analytical tools and interpreted the data; and T.M. designed research and wrote the paper.

Conflict-of-interest disclosure: The authors declare no competing financial interests.

Correspondence: Toshiyuki Miyata, National Cardiovascular Center Research Institute, 5-7-1 Fujishirodai, Suita, Osaka 565-8565, Japan; e-mail: miyata@ri.ncvc.go.jp.

References

1. Dong JF. Structural and functional correlation of ADAMTS13. Curr Opin Hematol. 2007;14:270-276.
2. Bergmeier W, Chauhan AK, Wagner DD. Glycoprotein Ibalpha and von Willebrand factor in primary platelet adhesion and thrombus formation: lessons from mutant mice. Thromb Haemost. 2008;99:264-270.
3. Tsai HM. Thrombotic thrombocytopenic purpura: a thrombotic disorder caused by ADAMTS13 deficiency. Hematol Oncol Clin North Am. 2007;21:609-632.
4. Zheng XL, Sadler JE. Pathogenesis of thrombotic microangiopathies. Annu Rev Pathol. 2008;3:249-277.
5. Desch KC, Motto DG. Thrombotic thrombocytopenic purpura in humans and mice. Arterioscler Thromb Vasc Biol. 2007;27:1901-1908.
6. Soejima K, Matsumoto M, Kokame K, et al. ADAMTS-13 cysteine-rich/spacer domains are functionally essential for von Willebrand factor cleavage. Blood. 2003;102:3232-3237.
7. Zheng X, Nishio K, Majerus EM, Sadler JE. Cleavage of von Willebrand factor requires the spacer domain of the metalloprotease ADAMTS13. J Biol Chem. 2003;278:30136-30141.
8. Ai J, Smith P, Wang S, Zhang P, Zheng XL. The proximal carboxyl-terminal domains of ADAMTS13 determine substrate specificity and are all required for cleavage of von Willebrand factor. J Biol Chem. 2005;280:29428-29434.
9. Majerus EM, Anderson PJ, Sadler JE. Binding of ADAMTS13 to von Willebrand factor. J Biol Chem. 2005;280:21773-21778.
10. Tao Z, Wang Y, Choi H, et al. Cleavage of ultra-large multimers of von Willebrand factor by C-terminal-truncated mutants of ADAMTS-13 under flow. Blood. 2005;106:141-143.
11. Tao Z, Peng Y, Nolasco L, et al. Recombinant CUB-1 domain polypeptide inhibits the cleavage of ULVWF strings by ADAMTS13 under flow conditions. Blood. 2005;106:4139-4145.
12. Gao W, Anderson PJ, Majerus EM, Tuley EA, Sadler JE. Exosite interactions contribute to tension-induced cleavage of von Willebrand factor by the antithrombotic ADAMTS13 metalloprotease. Proc Natl Acad Sci U S A. 2006;103:19099-19104.
13. Zhang P, Pan W, Rux AH, Sachais BS, Zheng XL. The cooperative activity between the carboxyl-terminal TSP1 repeats and the CUB domains of ADAMTS13 is crucial for recognition of von Willebrand factor under flow. Blood. 2007;110:1887-1894.

14. Banno F, Kaminaka K, Soejima K, Kokame K, Miyata T. Identification of strain-specific variants of mouse Adamts13 gene encoding von Willebrand factor-cleaving protease. J Biol Chem. 2004;279:30896-30903.
15. Zhou W, Bouhassira EE, Tsai HM. An IAP retrotransposon in the mouse ADAMTS13 gene creates ADAMTS13 variant proteins that are less effective in cleaving von Willebrand factor multimers. Blood. 2007;110:886-893.
16. Banno F, Miyata T. Biology of an antithrombotic factor-ADAMTS13. In: Tanaka K, Davie EW, eds. Recent Advances in Thrombosis and Hemostasis. Berlin, Germany: Springer; 2008:162-176.
17. Banno F, Kokame K, Okuda T, et al. Complete deficiency in ADAMTS13 is prothrombotic, but it alone is not sufficient to cause thrombotic thrombocytopenic purpura. Blood. 2006;107:3161-3166.
18. Miyata T, Kokame K, Banno F, Shin Y, Akiyama M. ADAMTS13 assays and ADAMTS13-deficient mice. Curr Opin Hematol. 2007;14:277-283.
19. Kokame K, Matsumoto M, Fujimura Y, Miyata T. VWF73, a region from D1596 to R1668 of von Willebrand factor, provides a minimal substrate for ADAMTS-13. Blood. 2004;103:607-612.
20. Kokame K, Nobe Y, Kokubo Y, Okayama A, Miyata T. FRETS-VWF73, a first fluorogenic substrate for ADAMTS13 assay. Br J Haematol. 2005;129:93-100.
21. Tsuji S, Sugimoto M, Miyata S, Kuwahara M, Kinoshita S, Yoshioka A. Real-time analysis of mural thrombus formation in various platelet aggregation disorders: distinct shear-dependent roles of platelet receptors and adhesive proteins under flow. Blood. 1999;94:968-975.
22. Chauhan AK, Motto DG, Lamb CB, et al. Systemic antithrombotic effects of ADAMTS13. J Exp Med. 2006;203:767-776.
23. Ni H, Denis CV, Subbarao S, et al. Persistence of platelet thrombus formation in arterioles of mice lacking both von Willebrand factor and fibrinogen. J Clin Invest. 2000;106:385-392.
24. Frenette PS, Moyna C, Hartwell DW, Lowe JB, Hynes RO, Wagner DD. Platelet-endothelial interactions in inflamed mesenteric venules. Blood. 1998;91:1318-1324.
25. DiMinno G, Silver MJ. Mouse antithrombotic assay: a simple method for the evaluation of antithrombotic agents in vivo. Potentiation of antithrombotic activity by ethyl alcohol. J Pharmacol Exp Ther. 1983;225:57-60.
26. Jackson SP. The growing complexity of platelet aggregation. Blood. 2007;109:5087-5095.
27. Konstantinides S, Ware J, Marchese P, Almus-Jacobs F, Loskutoff DJ, Ruggeri ZM. Distinct antithrombotic consequences of platelet glycoprotein Ibalpha and VI deficiency in a mouse model of arterial thrombosis. J Thromb Haemost. 2006;4:2014-2021.
28. Shida Y, Nishio K, Sugimoto M, et al. Functional imaging of shear-dependent activity of ADAMTS13 in regulating mural thrombus growth under whole blood flow conditions. Blood. 2008;111:1295-1298.
29. Smyth SS, Reis ED, Vaananen H, Zhang W, Coller BS. Variable protection of beta 3-integrin–deficient mice from thrombosis initiated by different mechanisms. Blood. 2001;98:1055-1062.
30. Cui J, Eitzman DT, Westrick RJ, et al. Spontaneous thrombosis in mice carrying the factor V Leiden mutation. Blood. 2000;96:4222-4226.
31. Weiler H, Lindner V, Kerlin B, et al. Characterization of a mouse model for thrombomodulin deficiency. Arterioscler Thromb Vasc Biol. 2001;21:1531-1537.
32. Suh TT, Holmback K, Jensen NJ, et al. Resolution of spontaneous bleeding events but failure of pregnancy in fibrinogen-deficient mice. Genes Dev. 1995;9:2020-2033.
33. Toomey JR, Kratzer KE, Lasky NM, Broze GJ Jr. Effect of tissue factor deficiency on mouse and tumor development. Proc Natl Acad Sci U S A. 1997;94:6922-6926.
34. Motto DG, Chauhan AK, Zhu G, et al. Shigatoxin triggers thrombotic thrombocytopenic purpura in genetically susceptible ADAMTS13-deficient mice. J Clin Invest. 2005;115:2752-2761.
35. Nishio K, Anderson PJ, Zheng XL, Sadler JE. Binding of platelet glycoprotein Ibalpha to von Willebrand factor domain A1 stimulates the cleavage of the adjacent domain A2 by ADAMTS13. Proc Natl Acad Sci U S A. 2004;101:10578-10583.
36. Shim K, Anderson PJ, Tuley EA, Wiswall E, Sadler JE. Platelet-VWF complexes are preferred substrates of ADAMTS13 under fluid shear stress. Blood. 2008;111:651-657.
37. Donadelli R, Orje JN, Capoferri C, Remuzzi G, Ruggeri ZM. Size regulation of von Willebrand factor-mediated platelet thrombi by ADAMTS13 in flowing blood. Blood. 2006;107:1943-1950.
38. Chauhan AK, Walsh MT, Zhu G, Ginsburg D, Wagner DD, Motto DG. The combined roles of ADAMTS13 and VWF in murine models of TTP, endotoxemia, and thrombosis. Blood. 2008;111:3452-3457.

Association of Asn221Ser mutation in tissue factor pathway inhibitor-β with plasma total tissue factor pathway inhibitor level

Junko Ishikawa[a], Hiromi Okada[a], Hisao Kato[a], Satoshi Takeshita[b], Shigenori Honda[a], Tomio Kawasaki[d], Etsuji Suehisa[e], Hajime Tsuji[f], Seiji Madoiwa[g], Yoichi Sakata[g], Tetsuhito Kojima[h], Mitsuru Murata[i], Yasuo Ikeda[j], Yoshihiro Kokubo[c], Tomonori Okamura[c], Hitonobu Tomoike[c] and Toshiyuki Miyata[a]

Tissue factor pathway inhibitor (TFPI) is an anticoagulant protease inhibitor that inhibits the tissue factor-initiated blood coagulation cascade reactions. Based on these anticoagulant functions of TFPI, we hypothesized that genetic variations in *TFPI* may alter the TFPI expression or impair the anticoagulant function and could predispose persons to deep vein thrombosis (DVT). This study was undertaken to examine whether the genetic polymorphisms in *TFPI* are associated with the plasma TFPI levels and risk for DVT. We sequenced the entire coding regions of *TFPI* in 175 Japanese DVT patients and identified 12 genetic variants, including one missense mutation, Asn221Ser. The missense mutation occurred at the site presumably attached to the glycosylphosphatidylinositol anchor in the TFPI-β form. The allele frequency of the mutant Ser-coding allele of the Asn221Ser mutation was 8% in the Japanese general population consisting of 1684 individuals. The Asn221Ser mutation was significantly associated with the total TFPI levels (Asn/Asn, $n = 108$, total TFPI $= 56.57 \pm 0.88$ ng/ml (mean ± SD) vs. Asn/Ser + Ser/Ser, $n = 16$, total TFPI $= 63.44 \pm 2.28$ ng/ml, $P = 0.0058$). The genotype was not associated with the free TFPI level. This Asn221Ser mutation was not associated with DVT. Thus, the Asn221Ser mutation occurring in the TFPI-β form was associated with the total TFPI level, but not a risk for DVT. The absence of the putative glycosylphosphatidylinositol anchor in TFPI-β under pathological conditions remains to be studied. *Blood Coagul Fibrinolysis* 20:22–26 © 2009 Wolters Kluwer Health | Lippincott Williams & Wilkins.

Blood Coagulation and Fibrinolysis 2009, 20:22–26

Keywords: deep vein thrombosis, glycosylphosphatidylinositol, tissue factor pathway inhibitor

[a]Research Institute, [b]Department of Medicine, [c]Department of Preventive Cardiology, National Cardiovascular Center, [d]Cardiovascular and Thoracic Surgery, Osaka University Graduate School of Medicine, [e]Laboratory for Clinical Investigation, Osaka University Hospital, Suita, [f]Division of Blood Transfusion and Cell Therapy, Kyoto Prefectural University of Medicine, Kyoto, [g]Center for Molecular Medicine, Jichi Medical University, Shimotsuke, Tochigi, [h]Department of Medical Technology, Nagoya University of School of Health Sciences, Nagoya, [i]Department of Laboratory Medicine and [j]Department of Internal Medicine, Keio University, Tokyo, Japan

Correspondence to Toshiyuki Miyata, PhD, National Cardiovascular Center Research Institute, 5-7-1 Fujishirodai, Suita, Osaka 565-8565, Japan
Tel: +81 6 6833 5012 ext. 2512; fax: +81 6 6835 1176;
e-mail: miyata@ri.ncvc.go.jp

Received 13 November 2007 **Revised** 13 March 2008
Accepted 27 March 2008

Introduction

Tissue factor pathway inhibitor (TFPI) is a protease inhibitor with three tandem Kunitz-type inhibitor domains, which inhibits the tissue factor-initiated blood coagulation cascade reactions by forming a complex with factor VIIa/tissue factor via the Kunitz-1 domain and with factor Xa via the Kunitz-2 domain [1–3].

The human TFPI gene resides on the long arm of chromosome 2 and has been originally reported as consisting of 9 exons [4–6]. Later on, an alternative spliced form, TFPI-β, was identified. Therefore, the human TFPI gene is now known to have 10 exons separated by 9 introns. Mature TFPI-α consists of 276 amino acid residues. An alternatively spliced form, TFPI-β, has a β-form specific C-terminal region encoded by exon 8 instead of the Kunitz-3 domain and the C-terminal region encoded by exons 9 and 10. The C-terminal region specific to the β-form directs the attachment of a putative glycosylphosphatidylinositol (GPI) anchor at Asn221, resulting in the formation of GPI-anchored TFPI-β [7–10]. TFPI-β thus formed is supposed to stay on the endothelial cell surface. Most TFPI-α are present in plasma, but some also stay on the endothelial cell surface through the heparan sulfate-binding sites on their Kunitz-3 domain and C-terminal region. TFPI binding to endothelium is considered to be important for the regulation of the initial phase of the coagulation cascade [1–3]. Although TFPI-α consisted 80% of TFPI on the cell surface, a recent study [11] suggests that TFPI-β was responsible for most of the cellular inhibitory activity for factor VIIa/tissue factor.

Animal models suggest the link of TFPI dysfunction or deficiency with a prothrombotic phenotype [12–15]. Mice lacking exon 4 of the *Tfpi* gene that encoded the

0957-5235 © 2009 Wolters Kluwer Health | Lippincott Williams & Wilkins DOI:10.1097/MBC.0b013e328304e0b9

Kunitz-1 domain ($Tfpi^{K1delta}$) showed embryonic lethality through hemorrhage due to a consumptive coagulopathy [12]. The lethal hemorrhagic phenotype for mice carrying the factor $VII^{-/-}$ genotype has been rescued by having $Tfpi^{K1delta}$ alleles [13]. Mice with a combined heterozygous *Tfpi* deficiency and homozygous apolipoprotein E deficiency ($Tfpi^{+/K1delta}$/apoE$^{-/-}$) exhibited a more pronounced atherosclerosis and thrombosis than mice with $Tfpi^{+/+}$/apoE$^{-/-}$ [14]. The $Tfpi^{K1delta}$ allele conferred the lethal thrombotic phenotype to mice homozygous for the factor V Leiden mutation [15].

Based on these anticoagulant functions of TFPI, we hypothesized that genetic variations within the *TFPI* gene may alter the TFPI expression or impair the anticoagulant function and could predispose persons to deep vein thrombosis (DVT). To test this hypothesis, we sequenced the entire coding region of the *TFPI* gene, including the TFPI-β-specific exon 8, in unrelated patients with objectively confirmed DVT for genetic variation and identified one novel missense mutation, Asn221Ser. This missense mutation occurred at an amino acid residue presumably attached with the GPI anchor in the TFPI-β form. By genotyping this mutation in a Japanese general population, we assessed the effects of the genotypes on the plasma TFPI levels and compared the genotype prevalence of the mutation in DVT patients with that in population-based controls. Finally, we found that the Asn221Ser mutation increased in the total TFPI levels but did not confer a genetic risk for DVT in our Japanese population. The Asn221Ser mutation was observed at a significant prevalence in the population, and the mutant TFPI-β was presumably not modified with the GPI anchor. Thus, functional analysis of the mutant form is needed to clarify the loss of the membrane anchoring of TFPI-β.

Materials and methods

Deep vein thrombosis patient group and general population

One hundred and seventy-five DVT patients were registered by the Study Group of Research on Measures for Intractable Diseases working under the auspices of the Ministry of Health, Labor and Welfare of Japan, as described previously [16,17]. The patients consisted of the previously enrolled 161 Japanese DVT patients and additional 14 DVT patients. Diagnosis of DVT was made by ultrasonography, radioisotope venography, and magnetic resonant imaging angiography. As the controls, a general population randomly selected from Suita city residents, the Suita Study, was used. The study design of the Suita Study has been described previously [18,19]. There were no exclusion criteria for the control individuals. A total of 1684 participants were included. The protocol of this study was approved by the Ethical Review Committee of each institute. Only those who gave written informed consent for genetic analyses were included in this study.

Direct DNA sequencing of tissue factor pathway inhibitor in deep vein thrombosis patients

We sequenced all 10 exons and flanking regions and 651 bp of the upstream region of exon 1 in *TFPI* in 175 DVT patients. The method of direct sequencing was described previously [20]. Information on the primers and PCR conditions is available upon request. The obtained sequences were examined for the presence of mutations using NAMIHEI (version 1.0; Mitsui Knowledge Industry, Tokyo, Japan) and Sequencher software (version 4.0; Gene Codes Corporation, Ann Arbor, Michigan, USA), followed by visual inspection [21]. We have adopted the mutation nomenclature recommendation, wherein the A of the ATG of the initiator Met codon is denoted nucleotide +1, and the initial Met residue is denoted amino acid +1 [22].

Genotyping of general population

The Asn221Ser (c.662A>G) genotyping was performed by the TaqMan allele discrimination method [21] using the primers 5′- CCACAGTGTTAAACATATAAAGATGACTCACA/5′-AACATGGATGCATGAATGCAGAAG and the probes 5′-VIC- CCGCATTCTTCCAAC (the wild-type Asn coding allele)/5′-FAM- CGCACTCTTCCAAC (the mutant Ser coding allele).

Measurement of plasma antigen levels of total and free tissue factor pathway inhibitor

The total TFPI antigen level was measured by the Total TFPI ELISA kit (Chemo-Sero-Therapeutic Research Institute, Kumamoto, Japan) [23]. The kit consisted of a rabbit anti-TFPI polyclonal antibody immobilized to the microplate well and a horseradish peroxidase-conjugated monoclonal antibody that can recognize the specific conformation formed between the Kunitz-1 and Kunitz-2 domains. The plasma antigen levels of free TFPI have been previously measured [24]. The antigen level of free TFPI was measured by a sandwich enzyme immunoassay method using the Kunitz-3 domain-specific monoclonal antibody [25]. The results were expressed as means ± one SD.

Statistical analysis

Pair-wise linkage disequilibrium between two polymorphisms was evaluated by determining r^2 with SNPAlyze software (version3.1; Dynacom, Mobara, Japan). The χ^2 test was used to compare the observed genotype frequencies with the Hardy–Weinberg equilibrium prediction. Comparisons between the case and control groups were analyzed by the χ^2 test using genotype and allele frequencies as independent variables. Association analyses in each sex of genotypes with plasma total and free TFPI levels were performed through logistic regression analysis considering the potential confounding

Table 1 List of genetic mutations identified in *TFPI* gene in 175 Japanese patients with deep vein thrombosis

Genomic	cDNA	Region	Amino acid change	Allele1 homo	Allele 1/2	Allele 2 homo	Total	Allele 1 frequency	Allele 2 frequency	Surrounding sequence	dbSNP ID
g.-51095C>T	c.-363-538C>T	promoter		66	78	31	175	0.60	0.40	ATTGT[C/T]TCACT	
g.-50983C>T	c.-363-426C>T	promoter		87	71	17	175	0.70	0.30	AAAAG[C/T]TTATT	rs10931292
g.-296G>A	c.-2-294G>A	intron2		110	59	6	175	0.80	0.20	TCAGC[G/A]TTTAC	rs2192824
g.-254T>C	c.-2-252T>C	intron2		173	2	0	175	0.99	0.01	ATATT[T/C]TCAAA	
g.6743G>A	c.174G>A	exon4	Ala58	174	1	0	175	1.00	0.00	AAGGC[G/A]GATGA	
g.19653T>C	c.628+8T>C	intron7		164	11	0	175	0.97	0.03	AAGAA[T/C]CTTGT	
g.19796_19799 GTTTdel	c.628+151_154 GTTTdel	intron7		139	29	7	175	0.88	0.12	AAATT[GTTT/---]AAGAC	rs8176613
g.24999A>G*	c.662A>G	exon8	Asn221Ser	149	25	1	175	0.92	0.08	GAAGA[A/G]TGCGG	rs7586970
g.25244T>C	c.847+60T>C	intron8		174	1	0	175	1.00	0.00	AAAAA[T/C]GAATA	
g.35804T>C	c.629-33T>C	intron8		149	25	1	175	0.92	0.08	TCACA[T/C]ATGGC	rs8176592
g.36030T>C	c.808+14T>C	intron9		173	2	0	175	0.99	0.01	GATAC[T/C]CTTCC	
g.37312T>A	c.1293+101T>A	3'flanking		128	45	2	175	0.86	0.14	TATAG[T/A]ATTCT	

Alleles 1 and 2 are major and minor alleles, respectively. * c.662A>G for the large scale genotyping by the TaqMan genotype discrimination method.The A of the ATG of the initiator Met codon is denoted nucleotide +1, and the initial Met residue is denoted amino acid +1, as recommended by the Nomenclature Working Group. The nucleotide sequence (GenBank Accession ID: NC_000002.10) was used as a reference sequence. c.-363-538C>T and c.-363-426C>T were previously designated as −399C>T and −287T>C, respectively.Linkage disequilibrium: c.662A>G and c.629-33T>C showed an r^2 of 1.00 and c.629-33T>C and c.1293+101T>A showed an r^2 of 0.22.

risk variable of age. Differences with P values less than 0.05 were considered statistically significant.

Results

Genetic polymorphisms in tissue factor pathway inhibitor gene in Japanese deep vein thrombosis patients

We sequenced all exons and flanking regions and 651 bp of the upstream region of exon 1 in *TFPI* in 175 DVT patients (Table 1). We identified 12 genetic variations, including c.662A>G in TFPI-β-specific exon 8 that encoded a missense mutation causing Asn221 to be replaced by Ser (Asn221Ser). This missense mutation occurred at the site presumably modified by the GPI anchor in the TFPI-β form. Among the 175 DVT patients, 25 were heterozygous carriers for the mutant Ser221-coding allele and one was homozygous. The allele frequency for the Ser221-coding allele was 0.077 in the DVT patients. This mutation, c.662A>G, was in complete linkage disequilibrium with c.629-33T>C.

Genotyping of Asn221Ser mutation in the general population and association with the plasma levels of total and free tissue factor pathway inhibitor and with deep vein thrombosis

We genotyped the Asn221Ser mutation in the general population consisting of 1684 individuals using the TaqMan allele discrimination method. The genotype was followed in the Hardy–Weinberg equilibrium ($P = 0.6894$). The minor G-allele frequency of c.662A>G (Asn221Ser) in the general population was 0.079. Next, we examined the effects of the genotype on the plasma TFPI levels. We found that the plasma total TFPI level was significantly elevated in individuals with the mutant Ser-coding allele (Asn/Asn, $n = 108$, total TFPI $= 56.57 \pm 0.88$ ng/ml (mean ± SD) vs. Asn/Ser + Ser/Ser, $n = 16$, total TFPI $= 63.44 \pm 2.28$ ng/ml, $P = 0.0058$; Table 2). This association was not found in men when the population was divided by sex. A free TFPI level was not associated with the genotype. Finally, we examined the association of this genotype with DVT. The allele frequency of the Ser221-coding allele in the general population group was not significantly different from that in the DVT patient group ($P = 0.888$; Table 3). The genotype frequency of the Asn221Ser mutation was not statistically different between the DVT patient group and the general population group. Thus, the Asn221Ser mutation in *TFPI* was not associated with DVT.

Discussion

In the present study, we resequenced 350 alleles of *TFPI* in 175 unrelated Japanese patients with objectively confirmed DVT for genetic variation and identified 12 genetic variations, including one missense mutation, Asn221Ser. We genotyped this missense mutation in the general population and examined the association of its genotype with plasma TFPI levels. We found that the Ser-coding allele was associated with the increased plasma level of total TFPI but not associated with the

Table 2 Association of plasma free and total tissue factor pathway inhibitor levels with Asn221Ser mutation

	Combined			Women			Men		
	n	Free TFPI[a] (ng/ml)	Total TFPI[a] (ng/ml)	n	Free TFPI[a] (ng/ml)	Total TFPI[a] (ng/ml)	n	Free TFPI[a] (ng/ml)	Total TFPI[a] (ng/ml)
Asn/Asn	108	16.0 ± 0.4	56.6 ± 0.9	47	15.1 ± 0.6	55.1 ± 1.2	61	16.7 ± 0.6	57.8 ± 1.3
Asn/Ser+Ser/Ser	16	16.3 ± 1.1	63.4 ± 2.3	6	13.4 ± 1.2	64.7 ± 3.3	10	17.7 ± 1.4	62.5 ± 3.2
P		0.783	0.006		0.342	0.007		0.522	0.164

TFPI, tissue factor pathway inhibitor. [a]Age adjusted.

Table 3 Numbers and genotype frequencies of *TFPI* c.662A>G mutation (Asn221Ser) in the control and deep vein thrombosis groups

	General population, number (%)	DVT group, number (%)
Genotypes*		
AA	1425 (84.6)	149 (85.1)
AG+GG	259 (15.4)	26 (14.9)
Total	1684 (100)	175 (100)
Allele frequency**		
A allele	3101 (92.1)	323 (92.3)
G allele	267 (7.9)	27 (7.7)
Total	3368 (100)	350 (100)

DVT, deep vein thrombosis; OR, odds ratio; TFPI, tissue factor pathway inhibitor. Comparisons between the DVT and the control groups were analyzed using a χ^2 test with the genotypes as independent variables (indicated by *P* and OR). *OR = 0.960 (0.620–1.486) Pearson $P = 0.855$: $\chi^2 = 0.033$, Fisher $P = 0.913$. **OR = 0.971 (0.643–1.466) Pearson $P = 0.888$: $\chi^2 = 0.020$, Fisher $P = 1.000$.

free TFPI level. Finally, we found that the missense mutation did not show the association with DVT.

TFPI is present in plasma as well as on the endothelium [1–3]. The anticoagulant function of TFPI on the endothelium is thought to be physiologically important. TFPI-α binds to heparin-like glycosaminoglycan on the endothelium through both the Kunitz-3 domain and the C-terminal tail [26], and TFPI-β is thought to bind to endothelium through its unique C-terminal GPI anchor [7–10]. The functional mutation, Asn221Ser, occurred at the putative site for the GPI anchor, and the Ser221 bearing mutant was presumed not to be GPI anchored. Therefore, it is a reasonable assumption that the mutant TFPI-β is released from the cell surface to the plasma, resulting in the increase in the plasma total TFPI antigen level.

There are several reports on the association of the genetic polymorphisms with the plasma TFPI levels. A polymorphism present in intron 7, named −33T>C in intron 7, identified in the French population, has been reported to show the association with plasma total TFPI levels and DVT [27,28]. Individuals with the CC genotype showed higher total TFPI levels than those with the TT genotype. The age-adjusted odds ratio for DVT associated with the CC vs. the TT genotype was 0.6. This polymorphism, −33T>C in intron 7, is c.629-33T>C in our study. By means of intensive DNA resequencing, we found that c.629-33T>C was in complete linkage disequilibrium with the Asn221Ser mutation ($r^2 = 1.0$; Table 1). The distance between the two is 10 806 bp. Thus, we considered −33T>C in intron 7 to be a mere marker and the Asn221Ser mutation to be a real functional variant for the increased plasma total TFPI level.

Several missense mutations, including Pro151Leu (Pro179Leu in the nomenclature of the initial Met as +1) and Val264Met (Val292Met in the nomenclature of the initial Met as +1) in the *TFPI* gene have been reported in the Europeans [29–37]; however, these mutations were not identified in the present study. The Pro151Leu mutation has been identified in 1.2% of German DVT patients [29] and 0.2% of German blood donors [30]. The mutation has been identified in 2.0% of Spanish DVT patients [31]. There were no heterozygotes for this mutation in the 211 UK DVT patients [32]. Thus, the sample size for the resequencing of *TFPI* in the present study may not be high enough to identify this mutation in our DVT population. The Val264Met mutation has been identified in 4.9% of the control French population [36], so if it were present in the Japanese population with the same frequency, we would have detected it in the present study. It is now well known that there are ethnic differences in the genetic background of thrombophilia. Factor V Leiden mutation and prothrombin G20210A mutation are established risk factors predominantly found in Caucasian population [38], and protein S K196E mutation is a risk factor in Japanese population [39]. The Val264Met mutation in the *TFPI* gene might be an ethnic specific genetic variation.

In this study, we revealed the presence of the Asn221Ser mutation in *TFPI* that presumably confers defects on the GPI anchor attachment. This mutation did not show the association with DVT, but influenced the plasma TFPI levels. Ser-coding allele-bearing individuals would have low anticoagulant potency on the endothelium. Thus, it may confer the predisposed prothrombotic phenotype under some pathophysiological conditions such as disseminated intravascular coagulation and restenosis after angioplasty. Further studies are needed to clarify the thrombotic risks predisposed by this mutation.

Acknowledgements

The authors declare no conflict of interest in connection with the submitted article.

The present study was supported by a Grant-in-Aid from the Ministry of Health, Labor, and Welfare of Japan, and the Ministry of Education, Culture, Sports, Science, and Technology of Japan, and the Program for Promotion of Fundamental Studies in Health Sciences of the National Institute of Biomedical Innovation (NIBIO) of Japan. Ms. Ishikawa was supported by Japan Health Sciences Foundation. Dr Okada was a postdoctoral fellow of Japan Cardiovascular Research Foundation.

References

1 Broze GJ Jr. Tissue factor pathway inhibitor and the revised theory of coagulation. *Annu Rev Med* 1995; **46**:103–112.

2 Kato H. Regulation of functions of vascular wall cells by tissue factor pathway inhibitor: basic and clinical aspects. *Arterioscler Thromb Vasc Biol* 2002; **22**:539–548.

3 Monroe DM, Key NS. The tissue factor-factor VIIa complex: procoagulant activity, regulation, and multitasking. *J Thromb Haemost* 2007; **5**:1097–1105.

4 Girard TJ, Eddy R, Wesselschmidt RL, MacPhail LA, Likert KM, Byers MG, *et al.* Structure of the human lipoprotein-associated coagulation inhibitor gene. Intro/exon gene organization and localization of the gene to chromosome 2. *J Biol Chem* 1991; **266**:5036–5041.

5 van der Logt CP, Reitsma PH, Bertina RM. Intron-exon organization of the human gene coding for the lipoprotein-associated coagulation inhibitor: the factor Xa dependent inhibitor of the extrinsic pathway of coagulation. *Biochemistry* 1991; **30**:1571–1577.

6 Enjyoji K, Emi M, Mukai T, Imada M, Leppert ML, Lalouel JM, *et al.* Human tissue factor pathway inhibitor (TFPI) gene: complete genomic structure and localization on the genetic map of chromosome 2q. *Genomics* 1993; **17**:423–428.

7 Ott I, Miyagi Y, Miyazaki K, Heeb MJ, Mueller BM, Rao LV, *et al.* Reversible regulation of tissue factor-induced coagulation by glycosyl phosphatidylinositol-anchored tissue factor pathway inhibitor. *Arterioscler Thromb Vasc Biol* 2000; **20**:874–882.

8 Mast AE, Acharya N, Malecha MJ, Hall CL, Dietzen DJ. Characterization of the association of tissue factor pathway inhibitor with human placenta. *Arterioscler Thromb Vasc Biol* 2002; **22**:2099–2104.

9 Zhang J, Piro O, Lu L, Broze GJ Jr. Glycosyl phosphatidylinositol anchorage of tissue factor pathway inhibitor. *Circulation* 2003; **108**:623–627.

10 Chang JY, Monroe DM, Oliver JA, Roberts HR. TFPIbeta, a second product from the mouse tissue factor pathway inhibitor (TFPI) gene. *Thromb Haemost* 1999; **81**:45–49.

11 Piro O, Broze GJ Jr. Comparison of cell-surface TFPIalpha and beta. *J Thromb Haemost* 2005; **3**:2677–2683.

12 Huang ZF, Higuchi D, Lasky N, Broze GJ Jr. Tissue factor pathway inhibitor gene disruption produces intrauterine lethality in mice. *Blood* 1997; **90**:944–951.

13 Chan JC, Carmeliet P, Moons L, Rosen ED, Huang ZF, Broze GJ Jr, *et al.* Factor VII deficiency rescues the intrauterine lethality in mice associated with a tissue factor pathway inhibitor deficit. *J Clin Invest* 1999; **103**:475–482.

14 Westrick RJ, Bodary PF, Xu Z, Shen YC, Broze GJ, Eitzman DT. Deficiency of tissue factor pathway inhibitor promotes atherosclerosis and thrombosis in mice. *Circulation* 2001; **103**:3044–3046.

15 Eitzman DT, Westrick RJ, Bi X, Manning SL, Wilkinson JE, Broze GJ, *et al.* Lethal perinatal thrombosis in mice resulting from the interaction of tissue factor pathway inhibitor deficiency and factor V Leiden. *Circulation* 2002; **105**:2139–2142.

16 Kimura R, Honda S, Kawasaki T, Tsuji H, Madoiwa S, Sakata Y, *et al.* Protein S-K196E mutation as a genetic risk factor for deep vein thrombosis in Japanese patients. *Blood* 2006; **107**:1737–1738.

17 Yin T, Takeshita S, Sato Y, Sakata T, Shin Y, Honda S, *et al.* A large deletion of the PROS1 gene in a deep vein thrombosis patient with protein S deficiency. *Thromb Haemost* 2007; **98**:783–789.

18 Mannami T, Baba S, Ogata J. Potential of carotid enlargement as a useful indicator affected by high blood pressure in a large general population of a Japanese city: the Suita study. *Stroke* 2000; **31**:2958–2965.

19 Kokubo Y, Inamoto N, Tomoike H, Kamide K, Takiuchi S, Kawano Y, *et al.* Association of genetic polymorphisms of sodium-calcium exchanger 1 gene, *NCX1*, with hypertension in a Japanese general population. *Hypertens Res* 2004; **27**:697–702.

20 Kokame K, Matsumoto M, Soejima K, Yagi H, Ishizashi H, Funato M, *et al.* Mutations and common polymorphisms in ADAMTS13 gene responsible for von Willebrand factor-cleaving protease activity. *Proc Natl Acad Sci U S A* 2002; **99**:11902–11907.

21 Kimura R, Kokubo Y, Miyashita K, Otsubo R, Nagatsuka K, Otsuki T, *et al.* Polymorphisms in vitamin K-dependent g-carboxylation-related genes influence interindividual variability in plasma protein C and protein S activities in the general population. *Int J Hematol* 2006; **84**:387–397.

22 den Dunnen JT, Antonarakis SE. Mutation nomenclature extensions and suggestions to describe complex mutations: a discussion. *Hum Mutat* 2000; **15**:7–12.

23 Kamikura Y, Wada H, Yamada A, Shimura M, Hiyoyama K, Shiku H, *et al.* Increased tissue factor pathway inhibitor in patients with acute myocardial infarction. *Am J Hematol* 1997; **55**:183–187.

24 Sakata T, Mannami T, Baba S, Kokubo Y, Kario K, Okamoto A, *et al.* Potential of free-form TFPI and PAI-1 to be useful markers of early atherosclerosis in a Japanese general population (the Suita Study): association with the intimal-medial thickness of carotid arteries. *Atherosclerosis* 2004; **176**:355–360.

25 Abumiya T, Enjyoji K, Kokawa T, Kamikubo Y, Kato H. An antitissue factor pathway inhibitor (TFPI) monoclonal antibody recognized the third Kunitz domain (K3) of free-form TFPI but not lipoprotein-associated forms in plasma. *J Biochem* 1995; **118**:178–182.

26 Enjyoji K, Miyata T, Kamikubo Y, Kato H. Effect of heparin on the inhibition of factor Xa by tissue factor pathway inhibitor: a segment, Gly212-Phe243, of the third Kunitz domain is a heparin-binding site. *Biochemistry* 1995; **34**:5725–5735.

27 Moatti D, Meirhaeghe A, Ollivier V, Bauters C, Amouyel P, de Prost D. Polymorphisms of the tissue factor pathway inhibitor gene and the risk of restenosis after coronary angioplasty. *Blood Coagul Fibrinolysis* 2001; **12**:317–323.

28 Ameziane N, Seguin C, Borgel D, Fumeron F, Moatti D, Alhenc-Gelas M, *et al.* The −33T−>C polymorphism in intron 7 of the TFPI gene influences the risk of venous thromboembolism, independently of the factor V Leiden and prothrombin mutations. *Thromb Haemost* 2002; **88**:195–199.

29 Kleesiek K, Schmidt M, Gotting C, Brinkmann T, Prohaska W. A first mutation in the human tissue factor pathway inhibitor gene encoding [P151L]TFPI. *Blood* 1998; **92**:3976–3977.

30 Kleesiek K, Schmidt M, Gotting C, Schwenz B, Lange S, Muller-Berghaus G, *et al.* The 536C−>T transition in the human tissue factor pathway inhibitor (TFPI) gene is statistically associated with a higher risk for venous thrombosis. *Thromb Haemost* 1999; **82**:1–5.

31 Gonzalez-Conejero R, Lozano ML, Corral J, Martinez C, Vicente V. The TFPI 536C−>T mutation is not associated with increased risk for venous or arterial thrombosis. *Thromb Haemost* 2000; **83**:787–788.

32 Evans GD, Langdown J, Brown K, Baglin TP. The C536T transition in the tissue factor pathway inhibitor gene is not a common cause of venous thromboembolic disease in the UK population. *Thromb Haemost* 2000; **83**:511.

33 Hessner MJ, Luhm RA. The C536T transition in the tissue factor pathway inhibitor (TFPI) gene does not contribute to risk of venous thrombosis among carriers of factor V Leiden. *Thromb Haemost* 2000; **84**:724–725.

34 Paciaroni K, Rossi E, Bazzan M, Ireland H, De Stefano V. Prevalence of the C536T mutation in the tissue factor pathway inhibitor (TFPI) gene among patients with venous thromboembolic disease. *Thromb Haemost* 2001; **85**:938–939.

35 Junker R, Glahn J, Tidow N, Brinkmann T, Nabavi DG. The tissue factor pathway inhibitor C536T mutation is not associated with the risk of stroke in young adults. *Thromb Haemost* 2002; **87**:920–921.

36 Moatti D, Seknadji P, Galand C, Poirier O, Fumeron F, Desprez S, *et al.* Polymorphisms of the tissue factor pathway inhibitor (TFPI) gene in patients with acute coronary syndromes and in healthy subjects: impact of the V264M substitution on plasma levels of TFPI. *Arterioscler Thromb Vasc Biol* 1999; **19**:862–869.

37 Arnaud E, Moatti D, Emmerich J, Aiach M, de Prost D. No link between the TFPI V264M mutation and venous thromboembolic disease. *Thromb Haemost* 1999; **82**:159–160.

38 Dahlback B. Progress in the understanding of the protein C anticoagulant pathway. *Int J Hematol* 2004; **79**:109–116.

39 Miyata T, Kimura R, Kokubo Y, Sakata T. Genetic risk factors for deep vein thrombosis in Japanese, importance of protein S K196E mutation. *Int J Hematol* 2006; **83**:217–223.

Acta Crystallographica Section F
Structural Biology and Crystallization Communications
ISSN 1744-3091

Masashi Akiyama,[a] Soichi Takeda,[a] Koichi Kokame,[a] Junichi Takagi[b] and Toshiyuki Miyata[a]*

[a]National Cardiovascular Center Research Institute, 5-7-1 Fujishirodai, Suita, Osaka 565-8565, Japan, and [b]Laboratory of Protein Synthesis and Expression, Institute for Protein Research, Osaka University, 3-2 Yamadaoka, Suita, Osaka 565-0871, Japan

Correspondence e-mail: miyata@ri.ncvc.go.jp

Received 17 April 2009
Accepted 18 June 2009

Production, crystallization and preliminary crystallographic analysis of an exosite-containing fragment of human von Willebrand factor-cleaving proteinase ADAMTS13

ADAMTS13 is a reprolysin-type metalloproteinase belonging to the ADAMTS (a disintegrin and metalloproteinase with thrombospondin type 1 motif) family. It specifically cleaves plasma von Willebrand factor (VWF) and regulates platelet adhesion and aggregation. ADAMTS13 is a multi-domain enzyme. In addition to the N-terminal metalloproteinase domain, the ancillary domains, including a disintegrin-like domain, a thrombospondin-1 type 1 repeat, a Cys-rich domain and a spacer domain, are required for VWF recognition and cleavage. In the present study, a fragment of the ADAMTS13 ancillary domains (ADAMTS13-DTCS; residues 287–685) was expressed using CHO Lec cells, purified and crystallized. Diffraction data sets were collected using the SPring-8 beamline. Two ADAMTS13-DTCS crystals with distinct unit-cell parameters generated data sets to 2.6 and 2.8 Å resolution, respectively.

1. Introduction

von Willebrand factor (VWF) is a plasma glycoprotein that is involved in platelet-dependent haemostasis (Sadler, 1998). VWF is primarily synthesized in vascular endothelial cells and megakaryocytes and is released into the plasma as ultralarge multimeric forms (UL-VWF) that are highly active in platelet adhesion and aggregation. A plasma metalloproteinase, ADAMTS13, specifically cleaves the Tyr1605-Met1606 peptidyl bond within the A2 domain of VWF (Dent *et al.*, 1990). Cleavage of UL-VWF into smaller forms by ADAMTS13 limits platelet thrombus formation. A deficiency of ADAMTS13 enzymatic activity caused by either genetic mutations in the ADAMTS13 gene or acquired autoantibodies against ADAMTS13 results in the accumulation of UL-VWF in plasma. This leads to the formation of disseminated platelet-rich microthrombi in arterioles, which is one of the characteristic pathogenic features of thrombotic thrombocytopaenic purpura (TTP), a life-threatening systemic disease (Tsai, 2009). Conversely, excessive cleavage of VWF causes von Willebrand disease type 2A (Sadler, 2005).

Human ADAMTS13 consists of 1427 amino acids and has a modular structure comprising a signal peptide, a short propeptide, a metalloproteinase domain (M), a disintegrin-like domain (D), a thrombospondin-1 type 1 repeat (T1), a Cys-rich domain (C), a spacer domain (S), seven additional type 1 repeats (T2–T8) and two CUB (C1r/C1s, urinary epidermal growth factor, bone morphogenic protein) domains (Levy *et al.*, 2001; Soejima *et al.*, 2001; Zheng *et al.*, 2001). C-terminal truncation of ADAMTS13 after the C but not the S domain results in severe loss of proteolytic activity towards VWF (Soejima *et al.*, 2003; Zheng *et al.*, 2003). Therefore, in addition to the M domain, the ancillary domains including the D, T, C and S domains (DTCS) are necessary for normal ADAMTS13 activity, although the distal C-terminal domains are required for regulation of *in vivo* thrombus formation under high-shear conditions (Banno et al., 2009). We have previously reported a minimal functional substrate consisting of 73 amino-acid residues of the C-terminal region of the VWF A2 domain (Asp1596–Arg1668) and designated VWF73 (Kokame *et al.*, 2004; Miyata *et al.*, 2007). A recent study has shown that the VWF-binding exosites located in the T, C and S domains interact with different segments of VWF73 (Gao *et al.*, 2008). These interactions increased the VWF-binding affinity and rate of substrate cleavage by

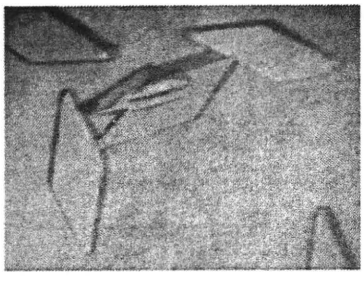

doi:10.1107/S1744309109023410

300-fold. At least 16 causative missense mutations for congenital TTP and five missense polymorphisms in the ADAMTS13 gene have been identified within the DTCS region (Levy *et al.*, 2001; Kokame *et al.*, 2002; Banno & Miyata, 2008). Although most TTP-causative mutant proteins are likely to show secretion deficiency, a P475S polymorphism variant showed normal secretion but reduced VWF-cleaving activity (Kokame *et al.*, 2002; Akiyama *et al.*, 2008). Detailed structural information on exosite-containing domains will help in understanding the structure-based mechanism of substrate recognition and specificity and the effects of TTP-causative mutations and common polymorphisms. To date, crystal structures of the M and D domains of three human ADAMTS-family proteins, ADAMTS1, ADAMTS4 and ADAMTS5, have been reported (Gerhardt *et al.*, 2007; Mosyak *et al.*, 2008; Shieh *et al.*, 2008). However, no crystal structures of exosite-containing fragments of ADAMTSs have been reported.

Here, we report the expression and purification of the exosite-containing human ADAMTS13-DTCS fragment using mammalian CHO Lec cells with mutations in multiple glycosylation-related genes. Proteins obtained from this cell line are suitable for crystallization because their restricted and homogeneous glycosylation improves the packing of the protein molecules. We also report the results of our crystallization and preliminary X-ray studies of ADAMTS13-DTCS.

2. Methods

2.1. Expression and purification of ADAMTS13-DTCS

An ADAMTS13 cDNA (AB069698) fragment corresponding to amino-acid residues 287–685 (ADAMTS13-DTCS) was amplified by PCR and cloned into a mammalian expression vector based on pcDNA3.1/Myc-His (Invitrogen), which has a mouse *Nid1* signal sequence (Yasui *et al.*, 2007). The nucleotide sequence was confirmed by dye-terminator sequencing. The ADAMTS13-DTCS fragment expressed from this vector contains a tobacco etch virus (TEV) proteinase cleavage site (Glu-Asn-Leu-Tyr-Phe-Gln/Gly) followed by tandem His-tag sequences at the C-terminus. We transfected the plasmid into CHO Lec 3.2.8.1 cells (Stanley, 1989) by electroporation and selected colonies resistant to G418 (3 mg ml^{-1}) on 96-well plates in α-minimal essential medium supplemented with 5% foetal bovine serum for 10 d. ADAMTS13-DTCS levels in the media of 48 G418-resistant colonies were examined by Western blotting with anti-6×His antibody (Sigma–Aldrich, St Louis, Missouri, USA). The clone with the highest secretion level of ADAMTS13-DTCS was cultured in the medium containing 0.5 mg ml^{-1} G418 by the roller-bottle method and the medium was collected every 3 d. The ADAMTS13-DTCS was recovered from the culture medium by 50%(*w*/*v*) ammonium sulfate precipitation and was purified by Ni–NTA agarose chromatography (Sigma–Aldrich). The eluted ADAMTS13-DTCS was incubated with TEV proteinase for 12 h at 297 K to remove the C-terminal tags. After dialysis in a buffer consisting of 10 m*M* MES and 100 m*M* NaCl pH 6.0, the digest was applied onto a Hi-Trap SP HP cation-exchange column (GE Healthcare, Buckinghamshire, England). The column was washed with the same buffer and ADAMTS13-DTCS was eluted with a linear gradient of NaCl (0.1–0.7 *M*) in 10 m*M* MES pH 6.0. Fractions were analyzed by SDS–PAGE under reducing conditions (Fig. 1). The fractions rich in ADAMTS13-DTCS (lanes 5 and 6) were combined, dialyzed against 10 m*M* MES pH 6.0 and concentrated using a Vivaspin-5 separation device (30 kDa molecular-weight cutoff; Sartorius, Edgewood, New York, USA) to a final concentration of ~10 mg ml^{-1} for crystallization.

2.2. Crystallization screening

Initial screening for crystallization conditions for ADAMTS-DTCS was carried out by the sitting-drop vapour-diffusion method using Index Screen, SaltRx Screen, PEG/Ion Screen, Grid Screen MPD and Grid Screen Ammonium Sulfate kits (Hampton Research, Aliso Viejo, California, USA). A volume of 0.1 µl protein solution was manually mixed with an equal amount of reservoir solution and the droplets were allowed to equilibrate against 0.1 ml reservoir solution at 293 K for 24 h.

2.3. Diffraction data collection

For X-ray measurements, crystals were soaked in a solution containing 20% glycerol, 26% PEG 1500, 100 m*M* MES pH 6.0 for cryoprotection prior to flash-freezing and were immediately exposed to a stream of nitrogen gas at 100 K. Preliminary X-ray data were collected using an in-house X-ray diffractometer (Micromax-007 X-ray generator with an R-AXIS VII imaging-plate detector; Rigaku, Tokyo, Japan) and diffraction-quality crystals were selected for data acquisition using the SPring-8 beamline. All the diffraction data sets were collected on beamline BL41XU at 100 K using an ADSC Quantum 310R detector and the diffraction images were processed using *HKL*-2000 software (Minor *et al.*, 2006).

3. Results and discussion

3.1. Protein preparation

We first attempted to express ADAMTS13-DTCS in *Escherichia coli* and insect cells. The expressed ADAMTS13-DTCS formed inclusion bodies and renaturation of ADAMTS13-DTCS did not succeed. We then tried to express ADAMTS13-DTCS in mammalian cells. As ADAMTS13-DTCS contains four potential N-glycosylation sites, we used the CHO Lec 3.2.8.1 cell line for stable expression. This cell line has four different mutated genes that are involved in the N- and O-glycosylation pathways (Stanley, 1989). Preliminary experiments showed that the endogenous signal and propeptide sequences of ADAMTS13 resulted in low protein secretion. We replaced the

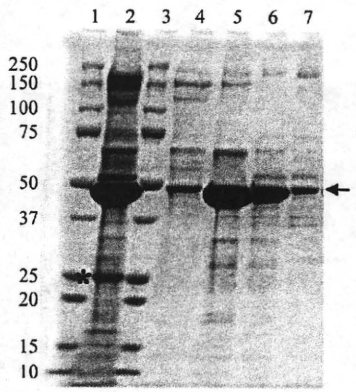

Figure 1
SDS–PAGE analysis of ADAMTS13-DTCS fractions from Hi-Trap SP HP cation chromatography. Proteins were analyzed by SDS–PAGE and stained with Coomassie Brilliant Blue. Lanes 1 and 3, molecular-weight markers (kDa); lane 2, pooled Ni–NTA eluate treated with TEV proteinase; lanes 4–7, eluate fractions Nos. 5–8, respectively, from the Hi-Trap SP HP column. Arrow, ADAMTS13-DTCS. Asterisk, TEV proteinase.

signal sequence and prosequence with the mouse *Nid1* signal sequence (Mann *et al.*, 1989). This replacement dramatically increased the secretion of ADAMTS13-DTCS into the medium. ADAMTS13-DTCS was purified by Ni–NTA chromatography followed by Hi-Trap SP cation-exchange chromatography. The molecular weight of the recombinant protein, 45 kDa, estimated by SDS–PAGE coincided well with the estimated molecular weight of 46 kDa (Fig. 1). Fractions (Fig. 1, lanes 5 and 6) from the Hi-Trap SP column were combined and used for crystallization without further purification. Approximately 6 mg ADAMTS13-DTCS was recovered from 20 l culture medium.

3.2. Crystallization

Of the 288 initial crystallization conditions tested, 20 yielded microcrystals (Fig. 2*a*). Using solution No. 4 of the PEG/Ion Screen kit [0.2 *M* lithium chloride, 20%(*w*/*v*) PEG 3350 pH 6.8] as a starting condition, the pH of the mother liquor, the concentration and molecular weight of the PEG and the species and concentrations of salts and additives were optimized. The combination of refinement of the crystallization conditions and an increase in the protein concentration (to ~20 mg ml^{-1}) improved the size of the crystals. Single crystals were obtained from drops made up of 0.5 µl protein solution and 0.5 µl reservoir solution [26%(*w*/*v*) PEG 1500, 100 m*M* MES pH 6.0] supplemented with a one-fifth volume of 40%(*w*/*w*) pentaerythritol ethoxylate (3/4 EO/OH; Additive Screen solution No. 52; Hampton Research). Crystals with dimensions of 300 × 100 × 50 µm were formed after 3–7 d at 293 K (Fig. 2*b*).

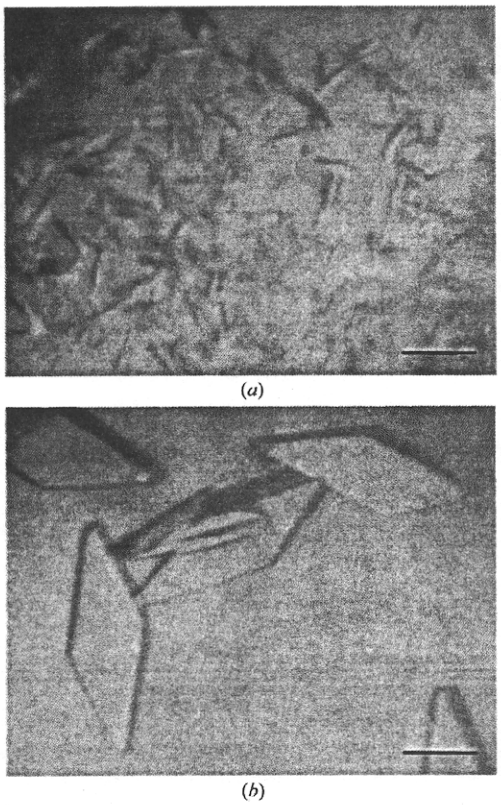

(*a*)

(*b*)

Figure 2
Crystals of human ADAMTS13-DTCS grown by the sitting-drop method. (*a*) Microcrystals obtained from solution No. 4 of the PEG/Ion Screen kit. (*b*) Crystals obtained using the optimized conditions. The scale bars indicate 0.1 mm.

Table 1
Data-collection statistics for ADAMTS13-DTCS crystals.

Values in parentheses are for the highest resolution shell. A single crystal was used for measurement for each data set.

	Form 1	Form 2
Space group	*C*2	*C*2
Unit-cell parameters		
a (Å)	152.7	138.6
b (Å)	52.9	51.4
c (Å)	76.2	76.4
β (°)	111.4	106.7
Wavelength (Å)	1.0	1.0
Resolution (Å)	50–2.60 (2.69–2.60)	30–2.80 (2.90–2.80)
No. of unique reflections	16867 (1272)	12811 (1259)
$R_{\rm merge}$†	0.052 (0.176)	0.062 (0.403)
$I/\sigma(I)$	19.3 (5.7)	13.3 (3.5)
Completeness (%)	95.3 (72.7)	99.5 (99.3)
Redundancy	3.5 (2.9)	3.7 (3.6)
Matthews value (Å^3 Da^{-1})	2.64	2.39
Solvent content (%)	53.4	48.6

† $R_{\rm merge} = \sum_{hkl}\sum_i |I_i(hkl) - \langle I(hkl)\rangle| / \sum_{hkl}\sum_i I_i(hkl)$, where $I_i(hkl)$ is the ith intensity measurement of reflection hkl and $\langle I(hkl)\rangle$ is its weighted average.

3.3. X-ray analysis

All diffraction data sets were acquired using the oscillation method on beamline BL41XU at a wavelength of 1.0 Å. The oscillation angle was 1.0° for all data sets. The native data sets for form 1 and form 2 contained 16 867 (2.60 Å resolution) and 12 811 (2.80 Å resolution) unique reflections, respectively. The asymmetric unit was estimated to contain one molecule, with corresponding crystal volume per protein weights of 2.7 and 3.1 Å^3 Da^{-1} for crystal forms 1 and 2, respectively. Solvent-content estimations based on a single copy of the molecule per asymmetric unit gave values of 53.4% and 48.6% for crystal forms 1 and 2, respectively. The X-ray data showed that the two crystal forms have different unit-cell parameters even when they are obtained under identical conditions. The variation in crystal packing might reflect the mobility of the domains in ADAMTS13-DTCS. The statistics of the data sets are summarized in Table 1.

3.4. Screening of heavy-atom derivatives

We attempted experimental phasing using heavy-atom derivatives because molecular replacement was not an option owing to the lack of related structures. The limited availability of single large crystals owing to the small amount of ADAMTS13-DTCS and its tendency to form multiple crystals produced difficulties in the search for heavy-atom derivatives. Therefore, we focused on investigating the colouring of crystals on heavy-atom soaking, which can be a good indication of heavy-atom binding. We selected 13 coloured compounds (Au-6, M1-10, M-11, M1-14, M1-15, M1-16, M1-17, M2-2, M2-3, M2-5, M2-16, M2-17 and M2-18) from Heavy Atom Screens (Hampton Research) and soaked small crystals in reservoir solution supplemented with each of these compounds. After several hours, we found that three osmium-containing compounds, ammonium hexabromoosmate (M2-16), potassium hexachloroosmate (M2-17) and osmium chloride (M2-18), were heavily absorbed into the crystals. To examine the X-ray diffraction from these potential derivatives, we prepared larger single crystals. We checked these using the in-house X-ray facility and well diffracting crystals were shipped for data acquisition at SPring-8. Structural analysis is now in progress using data obtained from the derivative soaked in the osmium chloride solution.

We thank M. Tomisako for her help with the crystallization experiments and Y. Ben Ammar and the staff of the SPring-8 beamline for assistance with the data acquisition. This work was supported in part by grants-in-aid from the Ministry of Health, Labour and Welfare of Japan, grants-in-aid from the Ministry of Education, Culture, Sports, Science and Technology of Japan, the Program for the Promotion of Fundamental Studies in Health Sciences of the National Institute of Biomedical Innovation (NIBIO) of Japan and a grant from the Takeda Science Foundation.

References

Akiyama, M., Kokame, K. & Miyata, T. (2008). *J. Thromb. Haemost.* **6**, 1830–1832.
Banno, F., Chauhan, A. K., Kokame, K., Yang, J., Miyata, S., Wagner, D. D. & Miyata, T. (2009). *Blood*, **113**, 5323–5329.
Banno, F. & Miyata, T. (2008). *Recent Advances in Thrombosis and Hemostasis*, edited by K. Tanaka & E. W. Davie, pp. 162–176. Tokyo: Springer.
Dent, J. A., Berkowitz, S. D., Ware, J., Kasper, C. K. & Ruggeri, Z. M. (1990). *Proc. Natl Acad. Sci. USA*, **87**, 6306–6310.
Gao, W., Anderson, P. J. & Sadler, J. E. (2008). *Blood*, **112**, 1713–1719.
Gerhardt, S., Hassall, G., Hawtin, P., McCall, E., Flavell, L., Minshull, C., Hargreaves, D., Ting, A., Pauptit, R. A., Parker, A. E. & Abbott, W. M. (2007). *J. Mol. Biol.* **373**, 891–902.
Kokame, K., Matsumoto, M., Fujimura, Y. & Miyata, T. (2004). *Blood*, **103**, 607–612.
Kokame, K., Matsumoto, M., Soejima, K., Yagi, H., Ishizashi, H., Funato, M., Tamai, H., Konno, M., Kamide, K., Kawano, Y., Miyata, T. & Fujimura, Y. (2002). *Proc. Natl Acad. Sci. USA*, **99**, 11902–11907.
Levy, G. G. *et al.* (2001). *Nature (London)*, **413**, 488–494.
Mann, K., Deutzmann, R., Aumailley, M., Timpl, R., Raimondi, L., Yamada, Y., Pan, T. C., Conway, D. & Chu, M. L. (1989). *EMBO J.* **8**, 65–72.
Minor, W., Cymborowski, M., Otwinowski, Z. & Chruszcz, M. (2006). *Acta Cryst.* D**62**, 859–866.
Miyata, T., Kokame, K., Banno, F., Shin, Y. & Akiyama, M. (2007). *Curr. Opin. Hematol.* **14**, 277–283.
Mosyak, L. *et al.* (2008). *Protein Sci.* **17**, 16–21.
Sadler, J. E. (1998). *Annu. Rev. Biochem.* **67**, 395–424.
Sadler, J. E. (2005). *Annu. Rev. Med.* **56**, 173–191.
Shieh, H. S., Mathis, K. J., Williams, J. M., Hills, R. L., Wiese, J. F., Benson, T. E., Kiefer, J. R., Marino, M. H., Carroll, J. N., Leone, J. W., Malfait, A. M., Arner, E. C., Tortorella, M. D. & Tomasselli, A. (2008). *J. Biol. Chem.* **283**, 1501–1507.
Soejima, K., Matsumoto, M., Kokame, K., Yagi, H., Ishizashi, H., Maeda, H., Nozaki, C., Miyata, T., Fujimura, Y. & Nakagaki, T. (2003). *Blood*, **102**, 3232–3237.
Soejima, K., Mimura, N., Hirashima, M., Maeda, H., Hamamoto, T., Nakagaki, T. & Nozaki, C. (2001). *J. Biochem.* **130**, 475–480.
Stanley, P. (1989). *Mol. Cell. Biol.* **9**, 377–383.
Tsai, H. M. (2009). *Kidney Int. Suppl.*, pp. S11–S14.
Yasui, N., Nogi, T., Kitao, T., Nakano, Y., Hattori, M. & Takagi, J. (2007). *Proc. Natl Acad. Sci. USA*, **104**, 9988–9993.
Zheng, X., Chung, D., Takayama, T. K., Majerus, E. M., Sadler, J. E. & Fujikawa, K. (2001). *J. Biol. Chem.* **276**, 41059–41063.
Zheng, X., Nishio, K., Majerus, E. M. & Sadler, J. E. (2003). *J. Biol. Chem.* **278**, 30136–30141.

Crystal structures of the noncatalytic domains of ADAMTS13 reveal multiple discontinuous exosites for von Willebrand factor

Masashi Akiyama[a,1], Soichi Takeda[a,1,2], Koichi Kokame[a], Junichi Takagi[b], and Toshiyuki Miyata[a,2]

[a]National Cardiovascular Center Research Institute, Suita, Osaka 565-8565, Japan; and [b]Laboratory of Protein Synthesis and Expression, Institute for Protein Research, Osaka University, Suita, Osaka 565-0871, Japan

Edited by Philip W. Majerus, Washington University Medical School, St. Louis, MO, and approved September 16, 2009 (received for review August 27, 2009)

ADAMTS13 specifically cleaves plasma von Willebrand factor (VWF) and thereby controls VWF-mediated platelet thrombus formation. Severe deficiencies in ADAMTS13 can cause life-threatening thrombotic thrombocytopenic purpura. Here, we determined 2 crystal structures of ADAMTS13-DTCS (residues 287–685), an exosite-containing human ADAMTS13 fragment, at 2.6-Å and 2.8-Å resolution. The structures revealed folding similarities between the disintegrin-like (D) domain and the N-terminal portion of the cysteine-rich domain (designated the C_A domain). The spacer (S) domain forms a globular functional unit with a 10-stranded β-sandwich fold that has multiple interaction sites with the C_A domain. We expressed 25 structure-based mutants of ADAMTS13-MDTCS (residues 75–685) and measured their enzymatic activity. We identified 3 VWF-binding exosites on the linearly aligned discontinuous surfaces of the D, C_A, and S domains traversing the W-shaped molecule. Since the MDTCS domains are conserved among ADAMTS family proteins, the structural framework of the multiple enzyme-substrate interactions identified in the ADAMTS13-VWF system provides the basis for a common substrate recognition mode in this class of proteinases.

hemostasis | metalloproteinase | modular protein | substrate recognition

The human ADAMTS (*a d*isintegrin-like *a*nd *m*etalloproteinase with *t*hrombo*s*pondin type-1 motif) family is composed of 19 genes that encode extracellular multidomain enzymes containing a reprolysin-type metalloproteinase domain and several conserved domains following the metalloproteinase domain (1). In contrast to the phylogenetically related ADAM (*a d*isintegrin *a*nd *m*etalloproteinase) family proteins, most of which have a transmembrane and a cytoplasmic domain in the C-terminal region (2), ADAMTSs are secretary proteinases that lack these domains and instead have at least 1 thrombospondin-1 (TSP-1) type-1 repeat (TSR). ADAMTSs have diverse functions including procollagen processing, aggrecan degradation, and organogenesis (1). ADAMTS13 controls platelet thrombus formation through cleavage of the von Willebrand factor (VWF).

VWF is a plasma glycoprotein that plays an essential role in platelet-dependent hemostasis (3, 4). VWF mediates platelet adherence to damaged blood vessels through interactions with glycoprotein Ib on the platelet surface and collagen in the subendothelium and contributes to platelet aggregation through interactions with integrin $\alpha_{IIb}\beta_3$. VWF, synthesized mainly in vascular endothelial cells, contains 2,050 aa residues and is released into the plasma as disulfide-bonded ultralarge VWF (UL-VWF) multimers having a mass greater than 20,000 kDa. In healthy individuals, UL-VWF multimers undergo limited proteolytic processing (5). ADAMTS13 specifically cleaves the Tyr-1605-Met-1606 peptidyl bond within the A2 domain of VWF (6) in a fluid shear-stress-dependent manner (7). Because VWF multimers have an alternate head-to-head and tail-to-tail disulfide-bonded architecture between neighboring subunits, cleavage by ADAMTS13 gives rise to a series of circulating multimers with molecular masses ranging from 500 to 15,000 kDa. Control of the size distribution of VWF multimers is important for normal hemostasis, as large multimers are hemostatically more active than small multimers (3). Deficiencies in ADAMTS13 activity, caused either by genetic mutations in the ADAMTS13 gene or by acquired inhibitory autoantibodies directed against the ADAMTS13 protein, results in the accumulation of UL-VWF in the plasma (8–11). The UL-VWF accumulation leads to the formation of disseminated platelet-rich microthrombi in the microvasculature, which results in the life-threatening disease, thrombotic thrombocytopenic purpura (TTP).

The human ADAMTS13 gene encodes a precursor protein of 1,427 aa with a modular structure consisting of a signal peptide, a propeptide (P), a metalloproteinase (M) domain, a disintegrin-like (D) domain, a TSR (T1), a cysteine-rich (C) region, a spacer (S), 7 TSRs (T2–T8), and 2 CUB (*c*omplement components C1rC1s/*u*rinary epidermal growth factor/*b*one morphogenetic protein-1) domains (11–13). The M domain of ADAMTS13 alone is not sufficient for recognition and specific cleavage of VWF, but full VWF-cleaving activity is achieved in vitro with an M-D-T1-C-S domain fragment (14–17). In addition, antibodies isolated from idiopathic TTP patients commonly inhibit ADAMTS13 activity by binding to the C and S domains of ADAMTS13 (14, 18, 19). Collectively, these observations indicate that the noncatalytic domains, especially the proximal C-terminal domains including the D, T1, C, and S domains (designated ADAMTS13-DTCS), are essential for recognition of VWF. The crystal structures of the MD domains (ADAMTS-MDs) of ADAMTS1 (20), ADAMTS4 (21), and ADAMTS5 (21) have been determined, but no structural information is currently available for the T1, C, and S domains of ADAMTS proteins. To gain insight into the molecular mechanism of VWF recognition by ADAMTS13, we solved the crystal structures of ADAMTS13-DTCS (residues 287–685) and performed a series of structure-based mutagenesis experiments to identify VWF-binding exosites. The present structure is the first for the TCS domains of any ADAMTS family member and will provide a template for understanding the role of these domains in substrate recognition by ADAMTS proteins.

Results

Structure Determination. The structure of ADAMTS13-DTCS was solved using the multiple-wavelength anomalous dispersion

Author contributions: M.A., S.T., K.K., J.T., and T.M. designed research; M.A. and S.T. performed research; M.A., S.T., and K.K. analyzed data; and M.A., S.T., and T.M. wrote the paper.

The authors declare no conflict of interest.

This article is a PNAS Direct Submission.

Data deposition: The atomic coordinates and structure factors have been deposited in Protein Data Bank, www.pdb.org [PDB ID codes 3GHM (form-1 ADAMTS13-DTCS) and 3GHN (form-2 ADAMTS13-DTCS)].

[1]M.A. and S.T. contributed equally to this work.

[2]To whom correspondence may be addressed. E-mail: stakeda@ri.ncvc.go.jp or miyata@ri.ncvc.go.jp.

This article contains supporting information online at www.pnas.org/cgi/content/full/0909755106/DCSupplemental.

www.pnas.org/cgi/doi/10.1073/pnas.0909755106

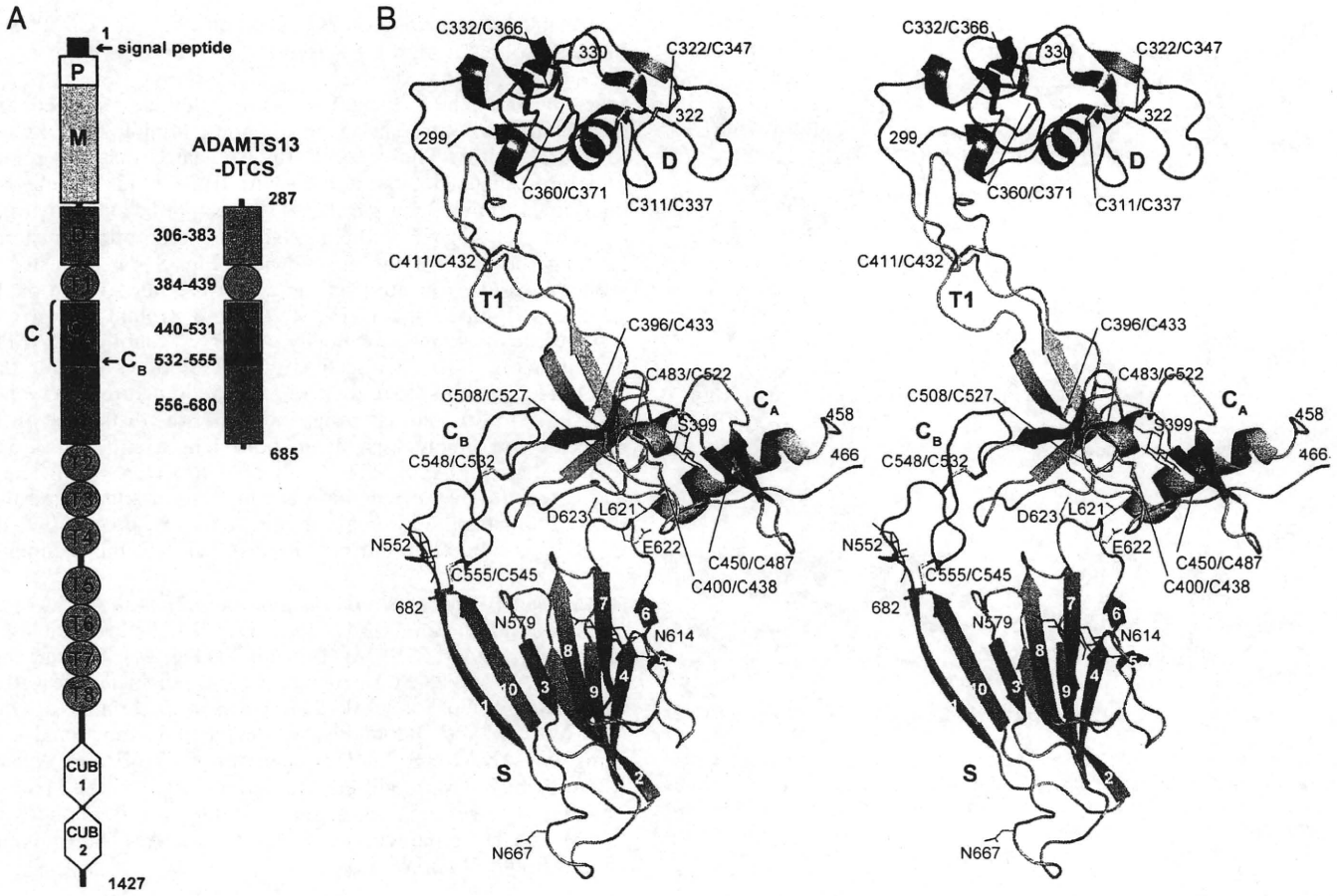

Fig. 1. Structure of ADAMTS13-DTCS. (*A*) Schematic representation of the domain structures of full-length ADAMTS13 and ADAMTS13-DTCS. (*B*) Ribbon structure of ADAMTS13-DTCS (form-1) in stereo. Domains are colored as in *A*. Strands in the S domain are numbered.

(MAD) method at 2.9 Å using data sets obtained from a single osmium derivative crystal (Table S1). The structure was further refined against 2 native data sets, form-1 (space group $C2$, a = 152.7 Å, b = 52. 9 Å, c = 76.2 Å, and β = 111.4°) and form-2 (space group $C2$, a = 138.6 Å, b = 51.4 Å, c = 76.4 Å, and β = 106.7°) at 2.6-Å (R = 0.243; R_{free} = 0.289) and 2.8-Å (R = 0.229; R_{free} = 0.280) resolution, respectively (Table S1). Each crystal contained 1 ADAMTS13-DTCS molecule per asymmetric unit. The final model of the form-1 (form-2) crystal includes ADAMTS13 residues 299–322 (323), 331 (330)-458, and 466–682. Electron densities for carbohydrate moieties attached to 3 of the 4 potential *N*-linked (Asn-552, Asn-579, and Asn-614) and one *O*-linked (Ser-399) site were observed (*SI Text* and Fig. S1). Pro-379, Pro-414, Pro-475, and Pro-618, were in the *cis* conformation.

Overall Structure. The N-terminal portion of the C domain (residues 440–531, designated the C_A domain here) in ADAMTS13 has a fold structurally homologous to that of the C domain of ADAMs, despite the lack of sequence similarity. The D domain (residues 306–383) of ADAMTS13 also has a fold similar to the C domain of ADAMs, which is consistent with recent crystallographic studies (20–22). Therefore, ADAMTS13 possesses 2 homologous domains that belong to the ADAM_CR family (Pfam database entry: pfam08516). The remaining C-terminal portion of the C domain (residues 532–555) is highly conserved in amino acid sequence among ADAMTS family proteins (Fig. S2, here called the C_B domain). The domain architecture of ADAMTS13 is schematically represented in Fig. 1*A*.

The overall structure of ADAMTS13-DTCS resembles a distorted W-shape, in which 3 knobs, the D, C_A, and S domains, are connected by 2 elongated structural modules, T1 and C_B (Fig. 1*B*). The homologous D and C_A domains are separated and related by a pseudo-90° screw rotation with an ≈45-Å translation along T1 (Fig. 1*B*). T1 has a very similar structure to that of the prototypical TSR, TSR2, in TSP-1 (23) with an rmsd of 1.37 Å for the equivalent Cα atoms (Fig. S1) and an antiparallel 3-stranded fold. Although the C_B domain has no apparent secondary structure, it has a series of turns stabilized by a pair of disulfide bonds (Cys-532-Cys-548 and Cys-545-Cys-555) and forms a rod shape with its N and C termini ≈25 Å apart (Fig. 1*B*). The C_A and S domains, bridged by the C_B domain, make direct contact through the extended loop of the S domain (Fig. 1*B* and *SI Text*). The structures of ADAMTS13 obtained from the 2 crystal forms are essentially the same, with the exception of the relative orientations between the domains (*SI Text* and Fig. S3). The structural details of the D, C_A, and S domains are described in the following sections and T1 in *SI Text*.

Comparison of the D and C_A Domains. The D and C_A domains have only 17% identity in their amino acid sequences (Fig. S2); however, their tertiary structures are quite similar (Fig. 2 *A*, *B*, and *E*). They share an N-terminal α-helix, 2 pairs of double-stranded antiparallel β-sheets, and 3 disulfide bonds, constituting the core structure of these domains. The D domain has an additional disulfide bond (Cys-322-Cys-347) that is strictly conserved among the ADAM counterparts (22, 24). The 3 peripheral loops differ markedly in structure between D and C_A in

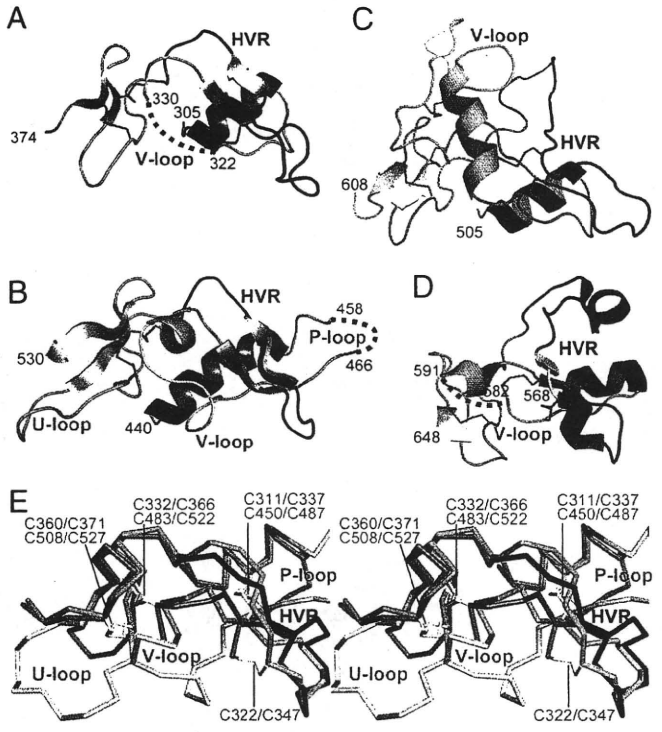

Fig. 2. Comparison of the D and C_A domain structures. Ribbon representation of the D (*A*) and C_A (*B*) domains of ADAMTS13-DTCS, and the C domains of VAP1 (representative of canonical ADAMs, PDB 2ERO) (*C*) and ADAM10 (PDB 2AO7) (*D*). The conserved α-helix, β-strands, and disulfide bonds are shown in red, yellow, and orange, respectively. The V-loop and HVR are shown in gray and blue, respectively. Disordered regions in the crystals are shown as dotted lines. The numbers of the terminal amino acid residues are indicated. (*E*) Superimposition of the D (orange) and C_A (green) domains in stereo. Disulfide bonds are indicated in stick representations.

ADAMTS13 (Fig. 2*E*). The amino acid sequences of these loops are also quite different between D and C_A in ADAMTS13 and in other ADAMTS family members (Fig. S2).

The loop following the first α-helix of the C_A domain (residues 454–469) is 12 aa residues longer than that of the D domain, protrudes from the main body of C_A, and is disordered along the distal side (Fig. 2 *B* and *E*). We designated this C_A-specific loop as the protruding (P) loop. One region in the D domain (residues 323–329) is disordered (Fig. 2*A*), not only in the current ADAMTS13 structures, but also in other reported ADAMTS1 structures (20), although the corresponding region of C_A is clearly defined in electron density maps. We designated this loop the variable (V) loop because of its variability in both length and amino acid sequence (Fig. S2). Canonical ADAM family members have a helix-loop insertion of 26–30 aa residues in the V-loop (Fig. 2*C*), whereas the atypical ADAM10 does not, and its C domain is more similar to the D and C_A domains of ADAMTS13, except for the hypervariable region (HVR) (Fig. 2*D*) (22, 24). ADAMTS13 has an insertion of 6 residues (residues 512–517) just before the C-terminal β-sheet of C_A (Fig. 2 *B* and *E*), which is not found in other ADAMTS members (Fig. S2). We designated this loop the ADAMTS13-C_A-unique (U) loop. Each C domain contains a HVR that differs markedly among ADAMs and may play a central role in substrate recognition (22, 24). ADAMTS13 has shorter HVRs in both the D and the C_A domains than those present in the ADAMs (Fig. 2 *A–D*). These loops and HVRs were targeted for mutations (see below).

There is an Arg-498-Gly-499-Asp-500 integrin recognition sequence in the C_A domain. The side chain of Arg-498 is buried and unavailable for protein–protein interactions, but the Asp-500 side chain is exposed toward the solvent.

Spacer Domain. The S domain is a long cysteineless segment and its primary structure shows no apparent homology to known structural motifs. The present study revealed that this region folds into a single globular domain with 10 β-strands in a jelly-roll topology, forming 2 antiparallel β-sheets that lie almost parallel to each other (Fig. 1*B* and Fig. S4*A*). The hydrophobic residues forming the core of the β-sandwich (Fig. S4*B*), a cluster of aromatic residues located on the concave outer surface of the smaller 4-stranded sheet (Fig. S4*C*), and proline and glycine residues in the loops, are highly conserved among ADAMTS proteins (Fig. S4*D*). Collectively, these findings suggest that ADAMTS proteins share the S domain architecture observed in ADAMTS13. In contrast, loops located at the distal side of the molecule are highly variable in both length and amino acid sequence among ADAMTS family members (Fig. S4*D*). The N and C termini of the S domain are in close proximity and thus the T2 following the S domain should be in close proximity to the C_A/S-domain junction but not the distal side of the S domain.

MDTCS Model. The reported crystal structures of the ADAMTS-MDs and our current ADAMTS13-DTCS structure enabled us to build an ADAMTS13-MDTCS model (Fig. 3*A*). The currently available ADAMTS-MD structures (20, 21) superimpose well on each other, except for subtle differences in the relative orientations of the M and D domains. We performed a functional assay using the ADAMTS13-MDTCS mutants F216E and A258C/K368C, which have modified interactions between the M and D domains. The results suggest that a stable association between the M and D domains is necessary for ADAMTS13 function (Fig. 3 *B* and *D* and *SI Text*).

VWF-Binding Exosites. We introduced mutations into ADAMTS13-MDTCS and measured the enzymatic activities of the mutants using the synthetic fluorogenic substrate FRETS-VWF73 (25). The results are summarized in Fig. 3 *C* and *D*.

In the current model, the D domain abuts the M domain catalytic site (Fig. 3*B*), suggesting that the surface of the D domain leading to the catalytic site functions as a VWF-binding exosite. Two mutants, 1 with a substitution in the HVR (D), R349D, and the other with 7 residues in the V-loop (D) replaced by a 4-residue linker, the ΔV-loop (D), exhibited diminished enzymatic activity (Fig. 3 *C* and *D*). The disordered V-loop (D) contains 4 charged residues, Arg-326, Glu-327, His-328, and Asp-330, which are suggested to lie in the vicinity of Arg-349 in the HVR (Fig. 3*B*). The cluster of these charged residues may collaboratively create an exosite (exosite-1). Charged amino acid-to-alanine substitutions revealed that Asp-1614, Glu-1615, and Lys-1617 in the VWF A2 domain act synergistically in ADAMTS13-mediated cleavage (26), suggesting that these charged residues in VWF are targets for exosite-1. Recently, Arg-349 was suggested to interact directly with VWF, most probably with Asp-1614 (27). Leu-350 and Val-352, which form a cluster of hydrophobic residues adjacent to the end of the catalytic cleft (Fig. 3*B*), also interact with VWF (27). This observation suggests that the hydrophobic cluster functions as a part of exosite-1.

The C_A domain has 3 surface loops. The ΔV-loop (C_A) mutant resulted in very low enzymatic activity (Fig. 3 *C* and *D*), suggesting that the V-loop (C_A) creates another exosite (exosite-2). A triple alanine substitution in the V-loop (C_A), H476A/S477A/Q478A, and a mutant at the N terminus of the HVR (C_A) adjacent to the V-loop (C_A), R488E, had significantly reduced activity (≈21%), suggesting that these hydrophilic or charged residues play a pivotal role in VWF recognition at exosite-2. The ΔU-loop and the F494Q/M496Q mutants showed reduced activity (≈40%) compared to the ΔP-loop mutant (≈53%). The

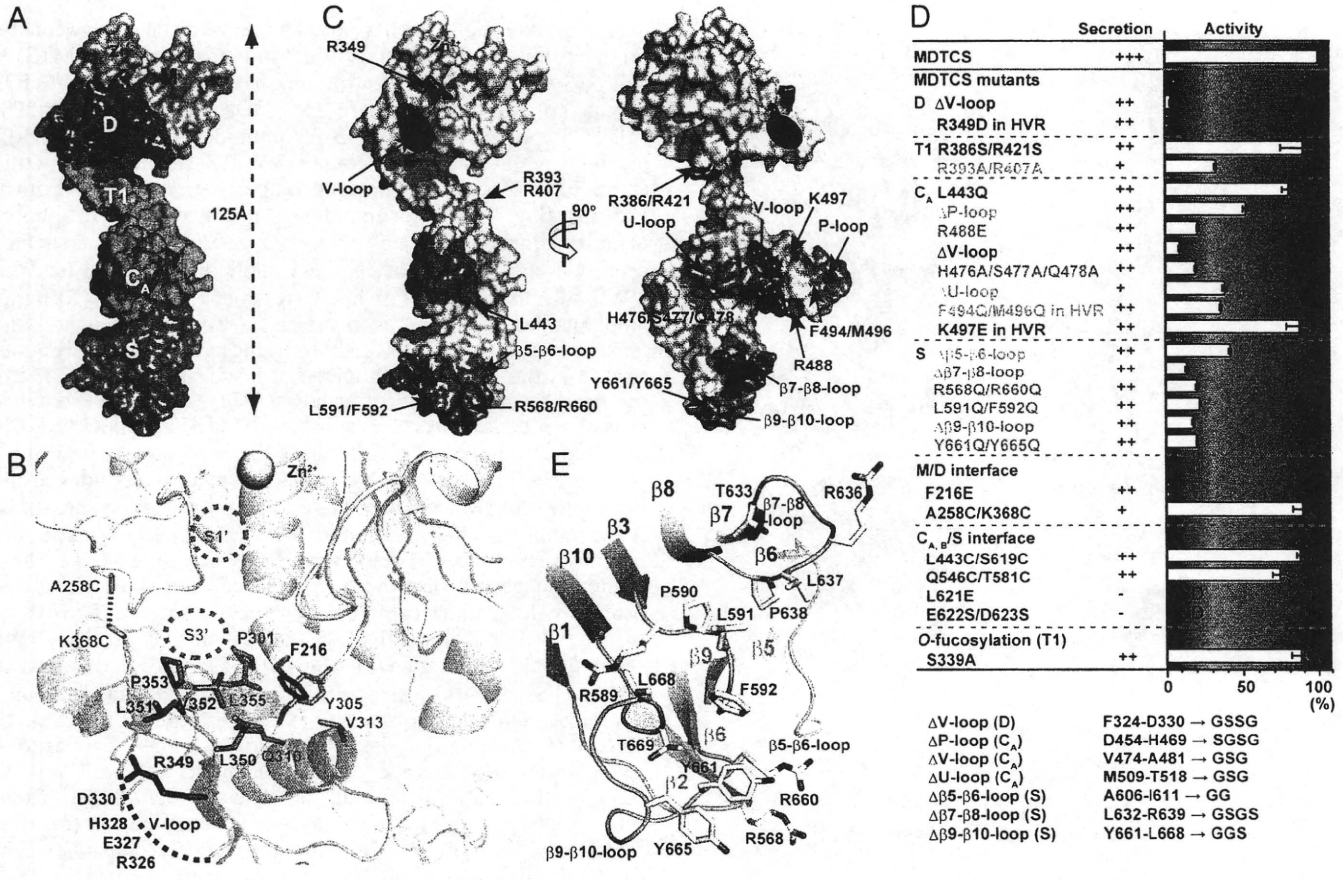

Fig. 3. A model of ADAMTS13-MDTCS and the residues affecting enzymatic activity. (*A*) Surface representation of the ADAMTS-MDTCS model. The M domain is shown in gray and the other domains are colored as in Fig. 1. The zinc ion is shown in yellow. (*B*) Close-up view of the interface between the M and D domains in the ADAMTS13-MDTCS model. Potential S1′ and S3′ substrate-binding sites, disordered V-loop (represented by a red dotted line), and the residues substituted by cysteine to form an interdomain disulfide bond (represented by a green dotted line) are indicated schematically. (*C*) The residues that affect ADAMTS13-MDTCS activity are indicated on the molecular surface, using a red-through-blue color-coding according to the results of the mutational assay shown in *D*. The molecule is viewed from 2 orthogonal directions. The V-loop of the D domain was disordered in the structures determined in this study and is represented by a red ellipsoid. (*D*) Summary of the mutational analysis, presenting the effects on secretion and enzymatic activity of the ADAMTS13-MDTCS mutants. Signs denote relative secretion level as follows: −, no detectable secretion; +, less than 30%; ++, 30≈70%; +++, 70∼100% of the secretion level of the wild type; ND, not determined. Relative enzymatic activities of the mutants are shown in the bar graph. The error bars indicate the range. (*E*) Close-up view of the hydrophobic cluster surrounded by arginine residues (exosite-3) in the S domain.

U-loop (C_A) and residues 494–496 flank the V-loop (C_A) and may contribute to exosite-2. In contrast, the P-loop is distant from the V-loop (C_A) and may contribute less to VWF binding. A mutation in the middle of the HVR (C_A), K497E, maintained enzymatic activity comparable to wild type, even though Lys-497 is the equivalent of Arg-349, the pivotal residue in exosite-1 in the homologous D domain.

The 3 distal loops in the S domain were replaced by short linkers and enzymatic activity in the mutants was assayed. The Δβ7-β8-loop and Δβ9-β10-loop mutants showed greatly reduced activity compared to the Δβ5-β6-loop mutant (Fig. 3 *C* and *D*). The β9-β10 loop contains 2 tyrosine residues, Tyr-661 and Tyr-665, which face the solvent. The Y661Q/Y665Q mutant was significantly less active (≈18%) than the wild type. These tyrosine residues and Leu-668 in the β9-β10 loop form a hydrophobic cluster together with residues in the neighboring β3-β4 and β7-β8 loops (Pro-590, Leu-591, Phe-592, Leu-637, and Pro-638) (Fig. 3*E*). Leu-591 and Phe-592 are located at the center of this hydrophobic cluster. The L591Q/F592Q mutant showed reduced activity (Fig. 3*D*). Four arginine residues surround the hydrophobic cluster (Fig. 3*E*). The R568Q/R660Q mutant was significantly less active than the wild type. Collectively, the hydrophobic cluster rimmed with arginine residues in the S domain may to be another VWF-binding exosite (exosite-3).

Mutations of residues (R386S/R421S and L443Q) located apart from the exosites and the *O*-linked fucosylation site (S339A) did not affect activity. The R393A/R407A mutation in T1 showed reduced activity (≈33%). Arg-407 is located at the bottom of a cleft formed between exosite-1 and exosite-2. This residue may also contribute to VWF binding.

Discussion

This study presents a structural determination of the ADAMTS13 DTCS domains, which constitute important functional part of the proteinase. The structure revealed that the residues important for stabilizing the DTCS core architecture are strictly conserved in all ADAMTS proteins. In contrast, peripheral loops within the D, C_A, and S domains were substantially different in both length and amino acid sequence among ADAMTSs, suggesting that these regions have specific functions that distinguish each ADAMTS member. By systematic mutagenesis, we identified 3 VWF-binding exosites in these loops (Fig. 3*C*). The exosites are highly conserved among ADAMTS13s from different species (Fig. S5). The 3 exosites were linearly aligned in the 3D structure, traversing the W-shaped ADAMTS13-DTCS molecule (Fig. 3*C*). This arrange-

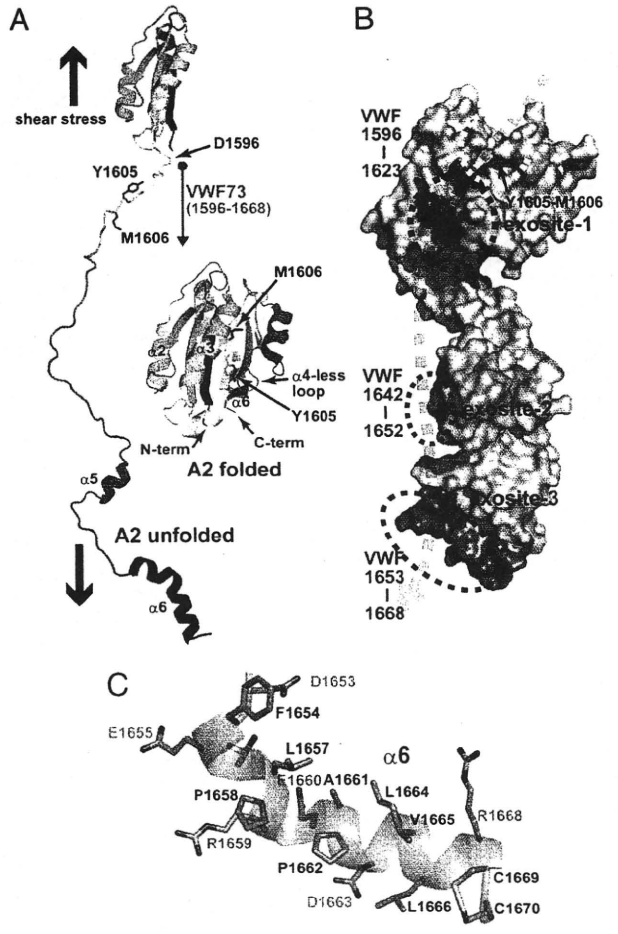

Fig. 4. ADAMTS13-VWF interactions. (*A*) Folded and unfolded structures of the VWF A2 domain. The VWF A2 domain adopts a Rossman fold with a central 6-stranded β-sheet surrounded by 5 α-helices (shown as "A2 folded") (28). The scissile peptide bond (Tyr-1605-Met-1606) is buried within the protein core under static conditions. The C-terminal region (residues 1,596–1,668, corresponding to VWF73) (31) of the A2 domain must be unfolded to expose the scissile bond and the exosite-binding regions under shear-stress conditions (shown as A2 unfolded). (*B*) ADAMTS13-MDTCS-VWF binding model. The molecular surface of the ADAMTS13-MDTCS model is shown in gray and the bound zinc ion is shown in yellow. Residues that mediate VWF binding are depicted as in Fig. 3C, and the exosites and the catalytic cleft are indicated by red and yellow dotted ellipsoids, respectively. The dotted green line represents a VWF molecule (residues 1,596–1,668) bound to ADAMTS-MDTCS. (*C*) Close-up view of the α6 helix and surrounding residues in the VWF A2 domain. Hydrophobic residues are indicated with red letters. Systematic charge-to-alanine substitutions revealed that the D1653A and D1663A mutations (cyan) reduced the substrate cleavage, the E1655A mutation (orange) slightly increased cleavage, and the R1659A, E1660A, and R1668A mutations (gray) had no significant effect (34).

ment suggests that these exosites bind collaboratively to multiple discontinuous regions of VWF.

A recent crystallographic study revealed that the Tyr-1605-Met-1606 scissile bond of VWF is buried within the core of the globular A2 domain under static conditions (Fig. 4*A*, A2 folded) (28). When VWF is subjected to fluid shear stress in circulation or denaturants in vitro, the A2 domain unfolds and adopts a partially extended conformation that makes its scissile peptide bond accessible for cleavage by ADAMTS13 (7, 29, 30) (Fig. 4*A*). We previously identified VWF73 (residues 1,596–1,668) as a minimum specific substrate for ADAMTS13 and suggested that a segment (residues 1,660–1,668) of VWF73 contains essential residues for recognition by ADAMTS13 (31). VWF73 is more than 200 Å long at its maximum extension, which is almost twice the distance between the catalytic site and the distal exosite-3 in the current ADAMTS13-MDTCS model. NMR spectroscopy has indicated that VWF73 adopts an unfolded structure (5). Therefore, the ADAMTS-MDTCS appears to be able to accommodate, by an induced-fit mechanism, a partially unfolded VWF73 segment along the extended molecular surface encompassing at least 3 critical exosites (Fig. 4*B*). Exosite-3 forms a cluster of hydrophobic residues rimmed by basic residues (Fig. 3*E*). Both the surface properties and the size of exosite-3 imply that exosite-3 binds to VWF, such that the VWF segment (residues 1,653–1,668) forms an amphipathic α-helix (α6 as in the crystal structure, Fig. 4*C*) and makes contact with ADAMTS13 by facing its hydrophobic residues toward exosite-3. Autoantibodies that inactivate ADAMTS13 are the most frequent cause of acquired TTP. These TTP patients possess antibodies directed against ADAMTS13 residues 657–666 (32) that exactly coincide with the β9-β10 loop, a part of exosite-3.

The present structure suggests a linear correspondence between the ADAMTS13 domains and their interaction sites in the A2 domain of VWF, consistent with previous systematic mutagenesis studies and kinetic analysis by Gao et al. (33). These authors suggested that the S domain contains an exosite that primarily determines catalytic efficiency by interacting with α6 of the VWF A2 domain (33). They identified 3 other VWF segments that interact with the MD, T1, and C domains of ADAMTS13 (17). Our structural and functional data are in good agreement with these observations, suggesting that the catalytic cleft plus exosite-1, exosite-2, and exosite-3 make cooperative, modular contacts with 3 discrete segments of the VWF A2 domain, the residues flanking the cleavage site (P9-P18′, residues 1,596–1,623), residues 1,642–1,652 and the α6 (residues 1,653–1,668) of the A2 domain, respectively (Fig. 4*B*). The model is also consistent with the previous observation that decreasing the length of peptides derived from the C terminus of the VWF A2 domain caused a progressive decrease in their potency as ADAMTS13 inhibitors (34). The elongated structure of the stiff, rod-like T1 module and its nonessential interactions with VWF (17) suggest that its primary role is to position the exosites spatially. The mobility of the domains (Fig. S3 and *SI Text*) suggests that a spectrum of ADAMTS13 conformations exist, with different spatial alignments of the exosites, increasing the possibility of ADAMTS13 interacting with partially unfolded VWF molecules, which also present a wide spectrum of conformations under shear-stress conditions in the circulation. The M domains of ADAMTS4 and ADAMTS5 do not retain specific catalytic activity. The inclusion of the proximal C-terminal domains enhances their aggrecanase activity, suggesting that these ADAMTSs function through multiple exosites (35–39), as observed in the ADAMTS13-VWF system.

More than 80 causative mutations for congenital TTP have been identified in the ADAMTS13 gene (11, 40, 41), including 16 missense mutations within the DTCS region. These mutations are not restricted to a specific region but are located throughout the molecule, suggesting that most of the mutations cause some structural defect that affects proper folding and secretion (Table S2). The R349C and P353L mutants, however, are likely to affect enzymatic activity: Arg-349 is in exosite-1 and Pro-353 forms part of the potential substrate-binding S3′ pocket (Fig. 3*B*). Five polymorphisms have been identified within the DTCS region (Table S2). Approximately 10% of the Japanese population are heterozygous for P475S substitution, located in the V-loop (C_A), which reduces VWF-cleaving activity (40, 42). The P618A substitution reduces secretion efficiency in cultured cells (43). Both proline residues adopt the *cis* conformation and, therefore, substitution by nonproline residues would cause structural distortions.

Shear stress in the blood circulation controls the exposure of the cryptic scissile bond and exosite-binding regions in VWF to ADAMTS13. The M domain of ADAMTS13 is catalytically